Computers and Structures 270 (2022) 106832

Contents lists available at ScienceDirect

Computers and Structures

journal homepage: www.elsevier.com/locate/compstruc

# Conjugate Bayesian updating of analytical fragility functions using dynamic analysis with application to corroded bridges

Yijian Zhang *, Iris Tien

*School of Civil and Environmental Engineering, Georgia Institute of Technology, Atlanta, GA, USA*

ARTICLE INFO

*Article history:*
Received 23 September 2021
Accepted 26 May 2022

*Keywords:*
Dynamic analysis
Structural finite-element models
Bayesian updating
Seismic fragility
Inspection data
Corrosion

ABSTRACT

Analytical fragility functions provide a way to quantify the risk of a structure. One method to construct seismic fragility curves is to perform a series of nonlinear dynamic analyses of the structure. As structural inspection data is increasing, updating fragility functions based on these measurements provides a way to translate collected data into risk-based decision-making support. However, the high computational cost in running and re-running analyses over the full finite-element model can be prohibitive. This paper presents a new methodology based on conjugate Bayesian updating to efficiently and accurately update analytical fragility curves. The reduction in computational cost from both reducing the number of analyses required and simplifying the structural complexity are investigated. The method is applied to update calculations of seismic bridge fragilities accounting for varying levels of measured corrosion. Results comparing updated fragility curves obtained from using the proposed approach versus using the full set of dynamic analyses show that the proposed method achieves accurate, stable, and more quickly converging fragility calculations. The number of structural analyses required is reduced by at least 60%, and the use of component-level analyses reduces computation time by 97% and more than an order of magnitude compared to existing methods.



## 1. Introduction

Fragility functions provide a way to quantify risk in structures under varying loading intensities. Functions represent the conditional probability of a structure exceeding a specific damage state *DS* given a realization *y* of intensity measure *IM* as shown in Eq. (1).

$$Fragility = Pr[DS|IM = y] \tag{1}$$

There are multiple methods of developing seismic fragility curves, including expert-based, empirical, experimental, analytical, and hybrid methods. The reader is referred to works such as Billah and Alam [9] for the advantages and disadvantages of the varying methods. This work focuses on analytical fragility curves as they can be developed in the absence of adequate actual damage data [9]. This includes developing fragilities over ranges of hazard intensities through conducting a series of numerical analyses. Researchers have combined seismic intensity and performance-based earthquake engineering concepts to create fragility curves to assess seismic structural performance in particular. For seismic fragility, variables in Eq. (1) become *DS* for damage state of the structural component under the earthquake, *IM* intensity measure of the ground motion, and *y* realization of ground motion intensity. Note that fragility assessment under other hazard types (e.g., flood, wind, etc.) is out of scope of this study. A review of fragility assessment for other hazard types can be found in Argyoudis et al. [5].

Analytical fragility curves are obtained through running either nonlinear time history analyses [14,46,48,50,64,65,65] or through incremental dynamic analysis on nonlinear finite-element models [36,58,38,62]. Fragility curves obtained from nonlinear time history analyses generate fragility assessments that are more reliable [55]due to the ability to consider various sources of uncertainty in the problem, including bridge geometries, material properties, and soil properties, during the dynamic analysis. It is, therefore, the method adopted in this paper.

However, there are several limitations in running nonlinear time history analyses to obtain analytical fragility curves. These relate to the high computational cost of the process, both in building the model and performing the analyses. The computational cost arises from needing to perform a sufficient number of dynamic analyses to obtain stable fragility assessments. The cost increases even further if the dynamic analyses are performed for

* Corresponding author.

https://doi.org/10.1016/j.compstruc.2022.106832
0045-7949/

high-fidelity finite-element models with large numbers of degrees of freedom and a high level of nonlinearity.

At the same time, structural inspection data is increasing, with monitoring systems measuring structural states becoming more widely used. The purpose of implementing structural inspection and structural health monitoring systems is to facilitate decision-making in the repair, rehabilitation, or replacement of structures. However, to do this, one must translate collected inspection data into decision-making support. One approach to effectively utilize inspection data to support structural management decisions is to update assessments of structural risk based on collected observations. Updating the fragility curves that quantify structural risk based on the collected data traditionally requires running a significant set of nonlinear time history analyses to reach convergence. These analyses must be re-run with each new collected observation. To investigate these converged results, there is still a debate among researchers about how many ground motions should be selected for generating reliable fragility curves [9]. As a result, researchers have proposed multiple methods to achieve reliable and converged estimates [7,34], where convergence indicates decreased sensitivity of the results to the consideration of additional ground motions in the analysis. This paper presents an alternative method to efficiently and accurately obtain the converged fragility estimate.

In addition, building the finite-element model itself, particularly for large and complex structural systems, can be burdensome due to complexities in structural geometries and boundary conditions. The cost for running each analysis also increases as the size and fidelity of the model increases. This paper proposes a methodology to address these limitations and provide a way to reduce the computational costs to obtain and update analytical fragility curves, e.g., based on collected inspection data and data from reduced numerical analyses, to assess structural risk. As more data is collected, the computational savings provided by the proposed method to update structural risk assessments based on new information enables newly collected data to be more efficiently and effectively utilized.

Bayesian techniques have been utilized to develop fragility curves in several previous studies. Singhal and Kiremidjian [56] combine building damage data on reinforced concrete buildings with fragility curves to arrive at more robust fragility assessments. Der Kiureghian [18] uses Bayesian methods to assess the fragility of electrical substation equipment based on field observations after an earthquake. Gardoni et al. [24] develop a methodology to construct probabilistic capacity models of structural components through a Bayesian updating approach based on observational data. Following that work, researchers have developed fragility estimates for reinforced concrete columns and bridges with two-column bents through a Bayesian methodology [12,63]. Koutsourelakis [33] combines Bayesian methods with Markov Chain Monte Carlo (MCMC) techniques to assess structural vulnerability using fragility surfaces. Mitropoulou and Papadrakakis [43] use a neural network to predict structural responses for fragility assessment in a significantly reduced computational time compared to that required by a conventional analysis. Li et al. (2013) [35] incorporate hybrid simulation with Bayesian updating techniques to improve the accuracy of the fragility function. Baker [7] proposes a framework for obtaining efficient analytical fragility functions through multiple stripe analysis procedures. Thanapol et al. [57] propose a procedure for updating the seismic reliability of existing reinforced concrete structures in a marine environment by incorporating the spatial steel corrosion distribution. Noh et al. [47] use conjugate Bayesian models to develop vulnerability functions combined with mortality rate data for treating the uncertainties in the earthquake. Kiani et al. [32] present a method for deriving fragility curves based on machine learning models. Sainct et al. [52] use active learning with support vector machine classifiers to estimate fragility curves. However, previous proposed methods, particularly those based on machine learning approaches, require sufficient amounts of data to proceed, including extensive datasets for training and testing, which is not required in the approach described in this paper. In addition, among prior studies, none consider the use of reduced models in the analyses, and none have been found to investigate the use of Bayesian updating techniques and conjugate Bayesian inference to reduce the computational cost required to create and update analytical fragility curves with a minimal number of structural analyses.

In the proposed method, updating rules from conjugate Bayesian inference are used to efficiently and accurately estimate fragility curves based on observational data with an analytically tractable posterior distribution. This is done by directly updating the fragility parameters with limited observational data rather than conducting the full set of analyses as is typically required. The observational data used in the proposed framework refers to the combination of corrosion-level measurements or other inspection data (e.g., mass loss of the steel reinforcement due to corrosion) and reduced finite-element simulation results (e.g., displacement ductility from the column response). The method is applied to assess the fragility of bridge structures in particular. With the idea of facilitating efficient and accurate fragility curve updating based on structural inspection data, the proposed method is applied to update a bridge column's fragility under varying levels of measured corrosion. Corrosion is a common inspection parameter of interest, particularly for reinforced concrete bridges [31]. The corrosion-level measurements for the observational data are measured by mass loss as one of the most widely recognized measures to explore and quantify the corrosion rate. The corrosion rate can be measured by electrical equipment, which can then be converted into a mass loss percentage using Faraday's law of electrolysis Broomfield, 2003; [27, 28]. The idea is to be able to generate and update analytical fragility curves based on new inspection information and a limited set of numerical data without needing to re-run the full set of analyses. The proposed method is evaluated both in terms of computational efficiency and accuracy of the resulting calculated fragilities. The current work puts emphasis on utilizing inspection data obtained from the field (e.g., mass loss due to corrosion) and simplified numerical data from a reduced finite-element model (e.g., displacement ductility from column response analyses) to efficiently and accurately update the fragility assessment. Results show two main advancements of the proposed method: (1) reduction in the number of structural analyses required to obtain stable fragility results, and (2) the ability to use reduced component-level analyses to update estimates of full structural performance.

The rest of the paper is organized as follows: the following two sections provide the theoretical basis for the relationship between fragility functions and the Bayesian updating approach in the methodology. The derivation of the fragility parameter updating rules using conjugate Bayesian inference is provided. The next section defines the prior distribution and observational data used for updating. Finally, to evaluate the proposed method's performance, the last two sections apply it to a full-bridge structure in the context of updating fragilities accounting for measured corrosion in the bridge column. First, observational data of the structural response from running nonlinear time history analyses considering the entire bridge based on a full structural finite-element model is considered. Second, more limited observational data from analyses of a reduced finite-element model of only a single column rather than the full structure is considered. In both cases, the accuracy of the resulting fragilities and the computational cost required to construct the fragility curves are investigated for the proposed approach compared to existing methods.

## 2. Definition of fragility function

In Eq. (1), the fragility is expressed explicitly as the probability of exceeding some damage state ($DS$) for a specific intensity measure ($IM$). The fragility function can also be expressed as the probability ($Pr$) of the demand, in this case seismic demand ($S_d$), exceeding the structural capacity ($S_c$) at a given intensity measure as shown in Eq. (2).

$$Fragility = Pr[S_d \geq S_c|IM] = Pr\left[\frac{S_d}{S_c} \geq 1|IM\right] \tag{2}$$

When both the demand and capacity distributions follow lognormal distributions, the fragility function has a closed-form solution. In this study, a classical lognormal fragility function is adopted [55,23,45,29,35]; Ghosh and Jamie, 2010; Li et al., 2013). While simulation-based approaches exist to assess seismic fragilities, the focus here is on generating analytical fragility curves. The probability of structural failure $P_f$ indicating the probability of the demand exceeding the capacity for a structural component is represented using parameters of the lognormal distributions of structural demand and capacity as shown in Eq. (3a). The reader is referred to Hwang et al. [30] and Melchers [42] for more details on the derivation of this solution. Alternatively, the fragility function can be expressed with respect to the ground motion intensity (e.g., peak ground acceleration or spectral acceleration) shown in Eq. (3b) [33].

$$P_f = \Phi\left(\frac{\ln\left(\frac{S_d}{S_c}\right)}{\sqrt{\xi_d^2+\xi_c^2}}\right) \tag{3a}$$

$$P_f = F(IM;\lambda,\xi) = \frac{1}{2} + \frac{1}{2}erf\left[\frac{\ln(IM)-\lambda}{\xi\sqrt{2}}\right] \tag{3b}$$

$\Phi(\cdot)$ is the cumulative distribution function of the standard normal distribution; $S_d$ and $S_c$ are the median parameters of the demand and capacity distributions, respectively; and $\xi_d$ and $\xi_c$ are the lognormal standard deviation parameters of the demand and capacity distributions, respectively. erf is an error function, $\xi$ is dispersion which is equal to $\sqrt{\xi_d^2+\xi_c^2}$, and $\lambda$ is the natural logarithm of the median ground motion intensity corresponding to unity of $\frac{S_d}{S_c}$. In the context of estimating the median demand from the probabilistic seismic demand models (PSDMs) using linear regression, Eq. (4) shows the estimate of the median of the demand distribution of the $m^{th}$ structural component by a power model [16].

$$S_{D,m} = a_m IM^{b_m} \tag{4a}$$

$$ln(S_{D,m}) = \ln(a_m) + b_m ln(IM) \tag{4b}$$

$\ln(a_m)$ and $b_m$ are the coefficients of the linear regression for the $m^{th}$ component. Together with Eq. (4), the fragility function shown in Eq. (3) can be expressed as shown in Eq. (5) [45].

$$P_f = \Phi\left(\frac{ln(IM)-\lambda_m}{\xi_m}\right) \tag{5a}$$

$$\lambda_m = \frac{\ln\left(S_{c,m}\right)-\ln(a_m)}{b_m} \tag{5b}$$

$$\xi_m = \frac{\sqrt{\xi_d^2+\xi_c^2}}{b_m} \tag{5c}$$

$\lambda_m$ is the lognormal mean for the $m^{th}$ component and $\xi_m$ its dispersion value.

## 3. Derivation of updating rules using conjugate Bayesian inference

The following equation gives a general framework of the Bayesian updating technique. It computes the posterior distribution of parameters $\boldsymbol{\theta}$ given new information ($\boldsymbol{X}$) obtained from collected experimental or numerical data [4].

$$f''(\boldsymbol{\theta}|\boldsymbol{X}) = kL(\boldsymbol{X}|\boldsymbol{\theta})f'(\boldsymbol{\theta}) \tag{6}$$

$k$ is a normalizing factor, $L(\boldsymbol{X}|\boldsymbol{\theta})$ the likelihood function, $f'(\boldsymbol{\theta})$ the prior distribution of parameter vector $\boldsymbol{\theta}$, and $f''(\boldsymbol{\theta}|\boldsymbol{X})$ the posterior distribution of parameter vector $\boldsymbol{\theta}$ given new information. To obtain an updated analytical fragility curve, the general idea is to update the original curve with new information through the Bayesian inference shown above, and the proposed method takes advantage of updating rules in conjugate Bayesian inference to estimate fragility curves combined with observational data. Within a Bayesian framework, both the original data and parameters that describe the distribution of the original data are treated as random variables. The original fragility data follows a lognormal distribution defined by its mean ($\lambda_m'$) and variance ($\xi_m'^2$). It is assumed that the mean ($\lambda_m'$) of the original fragility function is unknown, while the variance ($\xi_m'^2$) is known. This assumption holds within the study context where the original fragility function is known, and the objective is to efficiently update the estimated fragilities based on new information.

The following is the derivation of the updating rules. Let $\boldsymbol{Y}$ represent the original lognormal fragility data. $y_j$ represent independent sample points $1\cdots n$ from the original fragility curve as shown in Eq. (7).

$$y_j \; LN\left(\lambda_m', \xi_m'^2\right), j = 1\cdots n \tag{7a}$$

$$\ln(y_j) \; N\left(\lambda_m', \xi_m'^2\right), j = 1\cdots n \tag{7b}$$

From Eq. (2), the unknown parameter ($\boldsymbol{\theta}$) is chosen to be the unknown mean of the lognormal distribution ($\lambda_m'$). This is assumed to follow a normal distribution (Li et al., 2013) [34]. Analyses performed comparing results of the method using normal compared with lognormal prior distributions can be found in the appendix section. Other distributions may also be appropriate, but the performance of various prior distributions is out of the scope of this study, and can be considered for future work. The mean and standard deviation of the distribution are determined from the normal prior distribution of $\lambda_m'$ under a specified order of ground intensity measures. This process is discussed in more detail in the following section. Eq. (8) shows the normal prior distribution of the mean ($\lambda_m'$).

$$\lambda_m' \; N(\mu', \sigma'^2) \tag{8}$$

$\mu'$ is the mean of the normal distribution of the parameter ($\lambda_m'$) and $\sigma'^2$ its variance. From Eq. (2), one can show that the posterior distribution of the unknown parameter given observational data is proportional to the product of the likelihood and prior distribution as shown in Eq. (9).

$$f\left(\lambda_m'|\ln\left(\breve{y}\right)\right) \propto L\left(\ln\left(\breve{y}\right)|\lambda_m'\right)f\left(\lambda_m'\right) \tag{9}$$

$f\left(\lambda_m'|\ln\left(\breve{y}\right)\right)$ is the posterior distribution for $\lambda_m'$ conditioned on observational data, $f\left(\lambda_m'\right)$ is the prior distribution of $\lambda_m'$ which is assumed to be normally distributed, and $L\left(\ln\left(\breve{y}\right)|\lambda_m'\right)$ is the likelihood function conditioned on $n$ observational data points, which

can be represented by the product of probability density functions (PDFs) of the lognormal distribution evaluated at each new observational data point. $\ln\left(\breve{y}\right)$ is new information (e.g., displacement ductility of the column under a particular corrosion level). Observational data (e.g., observed mean of displacement ductility under a particular corrosion level) can then be computed by combining the new information, $\ln\left(\breve{y}\right)$, and the regression analysis shown in Eq. (5) and Eq. (6). Substituting the expression for the lognormal PDF into Eq. (9) results in Eq. (10). Note that the distributions are defined according to Bayesian probability theory and Bayesian inference, such that the posterior distribution is of the same type as the prior distribution and the prior is a conjugate prior for the likelihood function.

$$f\left(\lambda_m^{'}|\ln\left(\breve{y}\right)\right) \propto \exp\left(-\frac{1}{2}\frac{\sum_{i=1}^{n}\left(\ln\left(\breve{y}_i\right)-\lambda_m^{'}\right)^2}{\xi_m^{'2}}\right)\exp\left(-\frac{1}{2}\frac{\left(\lambda_m^{'}-\mu^{'}\right)^2}{\sigma^{'2}}\right) \quad (10)$$

Next, by introducing a new variable $n_o$, one can substitute $\xi_m^{'2}$ in Eq. (10) with the expression in Eq. (11) to obtain the result in Eq. (12).

$$\sigma^{'2} = \frac{\xi_m^{'2}}{n_o} \quad (11)$$

$$f\left(\lambda_m^{'}|\ln\left(\breve{y}\right)\right) \propto \exp\left(-\frac{1}{2}\frac{\sum_{i=1}^{n}\left(\ln\left(v_i\right)-\lambda_m^{'}\right)^2}{\xi_m^{'2}}\right)\exp\left(-\frac{1}{2}\frac{\left(\lambda_m^{'}-\mu^{'}\right)^2}{\frac{\xi_m^{'2}}{n_o}}\right) \quad (12)$$

$n_o$ represents the effective number of observations in the prior distribution [37]. Intuitively, $n_o$ captures information about the standard deviation of the prior distribution, as the magnitude of $n_o$ is inversely proportional to the prior standard deviation. The expression on the right-hand side of Eq. (12) can be further simplified to Eq. (13) by expanding terms and ignoring terms that do not depend on $\ln\left(\lambda_m^{'}\right)$.

$$f\left(\lambda_m^{'}|\ln\left(\breve{y}\right)\right) \propto \exp\left(-\frac{1}{\frac{2\xi_m^{'2}}{n+n_o}}\left(\lambda_m^{'}-\frac{n\ln\left(\bar{\breve{y}}\right)+n_o\mu^{'}}{n+n_o}\right)^2\right) \quad (13)$$

$\ln\left(\bar{\breve{y}}\right)$ is the mean value of $\ln\left(\breve{y}_i\right)$. The resulting updating rules for the parameters of the posterior distribution are as shown in Eq. (14).

$$\mu^{''} = \frac{n\ln\left(\bar{\breve{y}}\right)+n_o\mu^{'}}{n+n_o} \quad (14a)$$

$$\sigma^{''2} = \frac{\xi_m^{'2}}{n+n_o} \quad (14b)$$

$\mu^{''}$ and $\sigma^{''2}$ represent the mean and variance of the posterior distribution, respectively. Finally, the posterior-predictive distribution data ($\widehat{\boldsymbol{Y}}$) can be computed based on Eq. (15) assuming future data ($\widehat{\boldsymbol{Y}}$) is conditionally independent given $\lambda_m^{'}$.

$$f\left(\ln\left(\hat{y}\right)|\ln\left(\breve{y}\right)\right) = \int f\left(\ln\left(\hat{y}\right),\lambda_m^{'}|\ln\left(\breve{y}\right)\right)d\lambda_m^{'} \quad (15a)$$

$$f\left(\ln\left(\hat{y}\right)|\ln\left(\breve{y}\right)\right) = \int f\left(\ln\left(\hat{y}\right)|\lambda_m^{'}\right)\times f\left(\lambda_m^{'}|\ln\left(\breve{y}\right)\right)d\lambda_m^{'} \quad (15b)$$

With the recognition of the first and second terms on the right-hand side of Eq. (15b) to be the likelihood estimator and posterior distribution, respectively, further simplification of Eq. (15) leads to the sum of the two independent normal distributions as shown in Eq. (16) and parameters of the predictive-posterior distribution in Eq. (17).

$$f\left(\ln\left(\hat{y}\right)|\ln\left(\breve{y}\right)\right) = \mathrm{N}(\mu^{''},\ \xi_m^{'2}+\sigma^{''2}) \quad (16)$$

$$\lambda_m^{''} = \mu^{''} \quad (17a)$$

$$\xi_m^{''2} = \xi_m^{'2}+\sigma^{''2} \quad (17b)$$

In Eq. (17), $\lambda_m^{''}$ and $\xi_m^{''2}$ represent the mean and variance of the posterior-predictive distribution, respectively. In other words, these also refer to the mean and variance of the updated fragility function for the $m^{th}$ component. Note the current study assumes known variance and uses deterministic values assigned for the variance of the lognormal distribution to incorporate the conjugate Bayesian updating framework. The consideration of an additional distribution for the variance requires numerical techniques to solve for the desired variables, e.g., MCMC, which could decrease the efficiency of the proposed framework. The use of a known variance not only accelerates the Bayesian framework with minimal computational efforts but is also shown to provide accurate estimations.

## 4. Determination of parameters of prior distribution and observational data for Bayesian updating

Determining the parameters of the distribution of $\lambda_m^{'}$ requires a series of $\lambda_m^{'}$ sample points based on specified orders of the loading intensity measure, e.g., peak ground acceleration (PGA) for ground motion intensity in the assessment of seismic fragility. In the context of the probabilistic seismic demand model (PSDM), each new $\lambda_m^{'}$ is generated according to Eq. (4a) and Eq. (4b) by adding one numerical data point of displacement ductility at a time for the linear regression analysis. In general for PSDM, the ground motion intensity measures are generated randomly. This renders results with high randomness and influences the accuracy of the results. For example, if PGA values are ordered by increasing PGA, it overestimates the fragility; if data points are ordered by decreasing PGA, it underestimates the fragility. Therefore, in this study, the ground intensity measures are ordered such that the numerical data points start at the mean PGA value and oscillate around the mean with increasing deviation from the mean. This decreases the randomness in the outcome and results in a more robust method. While not all prior studies of fragility functions use ordered ground motions, for consistency in comparison in this study's results, the ordered ground motion approach is used in both the proposed and existing methods. Fig. 1 shows the PGA val-

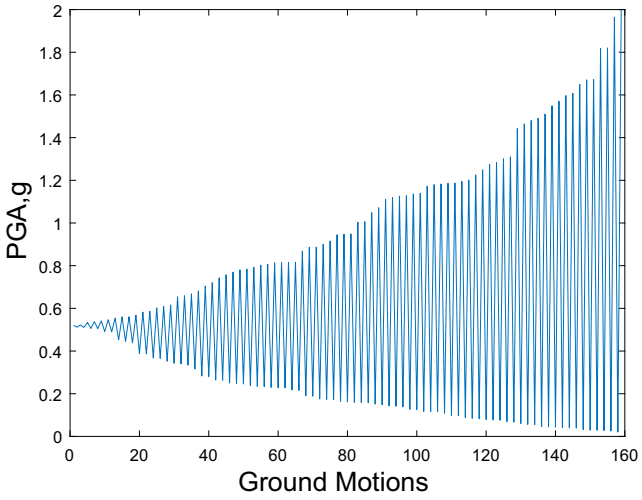


**Fig. 1.** Sequence of PGA values.

ues for a set of 160 ground motions that have been sequenced such that they follow the aforementioned order. Note that PGA is selected as the intensity measure (IM) over others due to its simplicity, ease of identification, and widespread use as an IM in seismic risk assessment [14]; Nielson and DesRoches, 2007 [46]; [29]. However, the proposed framework can also be incorporated with other IMs, such as the spectral acceleration at the first period $S_a(T_1)$. The accuracy and efficiency of using other IMs with the proposed framework would still hold compared to the existing approach.

The method of obtaining the series of $\lambda_m^{'}$ points for both the prior distribution and the observational data for Bayesian updating is the same. Once the prior distribution of $\lambda_m^{'}$ is specified, the mean and standard deviation of the prior distribution can be determined. Similarly, once assembly of the observational data is generated from the new information $\ln\left(\bar{y}\right)$, the updating rules as derived in the previous section can be applied to obtain the posterior distribution of $\lambda_m^{'}$.

The final step is to calculate the total sample variance ($\sigma_t$) of the predictive mean ($\lambda_m^{''}$) of the fragility function by combining the posterior-predictive variance and the standard deviation of the mean of observational data used for Bayesian updating by the square root of the sum of the squares (SRSS). The upper and lower bounds of the predictive mean ($\lambda_m^{''}$) are then computed accordingly. Rather than rendering a single value, the lower bound and upper bound of the posterior-predictive mean provide a range of possible values and corresponding confidence in the results. The bounds can be interpreted as capturing the epistemic uncertainty, with the confidence bounds becoming narrower as the number of observational data points increases.

The overall method is as shown in Fig. 2 and proceeds as follows: The first step is to obtain the original lognormal distribution with mean and variance $\lambda_m^{'}$ and $\xi_m^{'2}$, respectively, for the $m^{th}(m = 1, 2, 3, \cdots, n)$ component, where $n$ is the total number of critical components of the structure. The mean of the original lognormal distribution is assumed to follow a normal distribution with the mean and standard deviation of $\lambda_m^{'}$ computed based on the prior distribution as described in the previous section. Once the prior distribution is found, the updating rules (Eq. (14a) and (14b)) for normal conjugate pairs are applied to compute the posterior parameters. Parameters of the posterior-predictive distribution are then computed by summing the two independent normal distributions as shown from Eq. (15) to Eq. (17). The final confidence bounds on the result are then computed by SRSS. The same procedures are applied to the next structural component until it enumerates all the possible components in the structure. Note that the current study focuses on the bridge column response with the values of $m$ and $n$ set to be 1. The flowchart shown in Fig. 2 summarizes the procedures to obtain the final parameters for the updated fragility function.

## 5. Detailed Description of bridges with corrosion inspection data

To demonstrate and evaluate the proposed method to efficiently update fragility curves, it is applied to a sample bridge structure where the objective is to update the component fragility of the bridge column given observational data considering corrosion's effect.

### 5.1. Effect of corrosion

Multiple studies have shown the significant influence on steel's mechanical properties due to the effect of pitting corrosion [1,21,20,3]. In particular, Du et al. [21,20] have investigated the effects of pitting corrosion on steel bars' ductility and residual capacity. Kashani et al. [25] use 3D optical measurements of corroded bars to evaluate the spatial variability in corrosion patterns, and they have shown that the geometrical properties of corroded bars can be treated as a lognormal distribution. Meanwhile, several researchers [26,28,64] have adopted the aforementioned findings

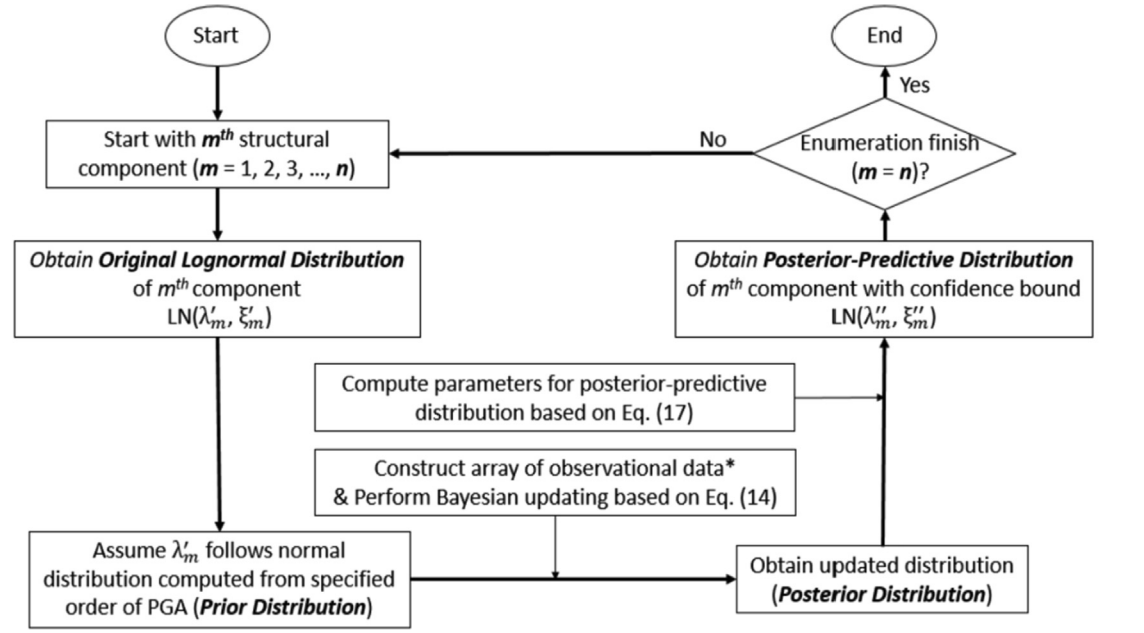


**Fig. 2.** Flowchart of the procedures to obtain the final parameters of the updated fragility function.

to account for the influence of pitting corrosion on the geometric properties of corroded steel bars with the mean values of a lognormal distribution. In this study, the main effect of corrosion on longitudinal reinforcement is captured by modifying the geometric and constitutive behavior of the longitudinal reinforcement, which accounts for inelastic buckling and ductility loss [26]. The corrosion effect on reinforcement in reinforced concrete bridge structures is represented by applying the average reductions in diameter of reinforcement and yield strength as shown in Eq. (18) and (19), respectively.

$$d_{b\_cor} = \frac{d_b}{10}\sqrt{100 - \psi} \tag{18}$$

$$f_{y\_cor} = f_y(1 - \beta\psi) \tag{19}$$

$d_{b\_cor}$ and $d_b$ are the corroded and pristine diameter of longitudinal bars, respectively; $f_{y\_cor}$ and $f_y$ are corroded and pristine yield strength of steel bar, respectively; $\psi/100$ is mass loss ratio measuring the level of corrosion; $\beta$ is pitting coefficient. Meanwhile, the influence of corrosion on concrete cracking is modeled based on modified compression field theory [59], as shown in Eq. (20).

$$f_{cr} = \frac{f_c}{1+K\frac{\varepsilon_1}{\varepsilon_{co}}} \tag{20}$$

$f_{cr}$ and $f_c$ are reduced concrete strength due to cracking and pristine compressive concrete strength, respectively; $K$ is coefficient related to bar roughness and diameter with a value of 0.1 [10]; and $\varepsilon_{co}$ and $\varepsilon_1$ are the strains of the peak concrete compressive strength and smeared tensile strain in the cracked concrete with right angles to the direction of the compression, respectively. There is a reduction of strength and stiffness of the concrete constitutive behavior in compression due to transverse tensile strain. This theory has been applied to corroded reinforced concrete beams to capture the effect of cracked concrete cover [17]. Concrete cracking and spalling in compression can be described by reduced strength in the concrete constitutive behavior described in Eq. (20). The average tensile strain in Eq. (20) is contingent on the magnitude of the total crack width. Eq. (21) proposed by Molina et al. [44] gives a relation between total crack width ($w_{cr}$) and depth of the corrosion attack ($X$), assuming all corrosion products accumulate around the reinforcement.

$$w_{cr} = 2\pi(\upsilon_{rs} - 1)X \tag{21}$$

$\upsilon_{rs}$ is the ratio of volumetric expansion of the oxides with respect to the virgin material. The depth of the corrosion attack can then relate to corrosion quantification (i.e., mass loss), which is discussed in detail by Shang et al. [54]. While the corrosion does affect the bond strength of the corroded vertical reinforcement, previous studies (Ou et al., 2012; [60,61,2,28] have found that the reduced bond strength does not govern the failure of the corroded column based on observed experimental results. Instead, the failure of columns under cyclic loading is mainly governed by other failure modes, such as fracture of bars in tension, buckling of bars, etc. For the behavior of core concrete considering the effect of corrosion, there is still no clear evidence to quantify the impact of corrosion. However, previous studies account for the effect of corrosion on the constitutive behavior of core concrete by considering premature fracture of transverse reinforcement due to corrosion (Kashani et al., 2016) [28], which leads to the crushing of confined concrete due to the first fracture of the spiral [68]. This behavior is included in this study.

Combining all effects, Fig. 3 shows the material stress–strain behavior of the (a) core concrete, (b) cover concrete, and steel bar in (c) tension, and (d) compression of a circular reinforced concrete column considering the effect of corrosion. Behavior under varying degrees of corrosion are shown. Corrosion is indicated by percent mass loss of both transverse and longitudinal steel reinforcement, and different degrees of cracking are described.

### 5.2. Description of sample bridge

The sample bridge is a typical multi-continuous concrete box girder bridge [50], with longitudinal and transverse views shown in Fig. 4. In addition to ground motion uncertainties, this study has accounted for the uncertainties in the selected bridge's geometric and material properties [50,64]. Table 1a summarizes the mean and variance values of the geometric parameters with lognormal distributions as indicated in Fig. 3 based on an extensive review of bridge plans. Table 1b summarizes the distributions of key mechanical and material properties of the bridge. The sample bridge consists of two spans and a single column bent with an integral type connection. The bridge employs a circular column supported on a pile cap with a group of piles underneath it. The column consists of #11 longitudinal rebars and #4 stirrups with 75 mm spacing on center. The bridge girders are cast-in-place prestressed concrete boxes with 0.04 for depth-to-span ratios. The bridge deck is seated on the elastomeric bearing pad at the abutments consisted of a 1.8 m tall backwall and Class 70 piles with a spacing of 2 m on center. Note the selection of this simpler bridge type is to illustrate the implementation of the proposed methodology, and the proposed methodology can also apply to more complex structures consisting of up to $n$ critical structural components.

The 3-D numerical model of the bridge is built in the finite-element software OpenSees (McKenna, 1997) [69]. The models are developed by sampling across the parameters listed in Table 1 through the method of Latin Hypercube Sampling (LHS) [40]. The uncertainty in material parameters listed in Table 1b is summarized by Ramanathan [50]. For example, the compressive strength of the concrete follows the recommendations of Choi [13], which is modeled using a normal distribution. The yield strength of reinforcement follows a lognormal distribution recommended by Ellingwood and Hwang [22].

For modeling the bridge column, a single column with two force-based beam-column elements connected in series is used in this study, as shown in Fig. 5. The column is assumed to have double curvature with an inflection point at the middle node [64], and strain penetration effects [67] have also been considered. Each force-based beam-column element consists of three integration points with fiber discretization to capture the flexural response. With this number of integration points, there are minimal issues with strain localization in relation to the structural response. However, if desired, an alternative way to tackle strain localization is through implementing regularization approaches [15,65,65]. For uniaxial material models, the 'Concrete02' material model is used for the behavior of the concrete, and the confinement effect in the column is captured through treatment of the stress–strain behavior of the uniaxial fiber in the confined region [39]. The 'Steel01' material with a uniaxial bilinear steel model is used to capture the hardening effect in the reinforcement.

The foundation consists of calibrated rotational and translational springs. For the superstructure, the bridge deck is modeled using equivalent elastic beam-column elements under the assumption that the bridge deck remains linearly elastic during seismic events. Shear keys are located at the abutments. They are modeled using zero-length elements with a maximum displacement of 3.5 in [41]before the corresponding shear capacity reduces to zero to capture the nonlinear backbone response. Based on pre-1971 design criteria in California for which this bridge type is common [50], the seat-type abutment is used in the bridge model. The longitudinal response of the abutment includes two types of resistance, passive and active. Passive resistance considers resistance contributed by the soil backfill and abutment pile, whereas active

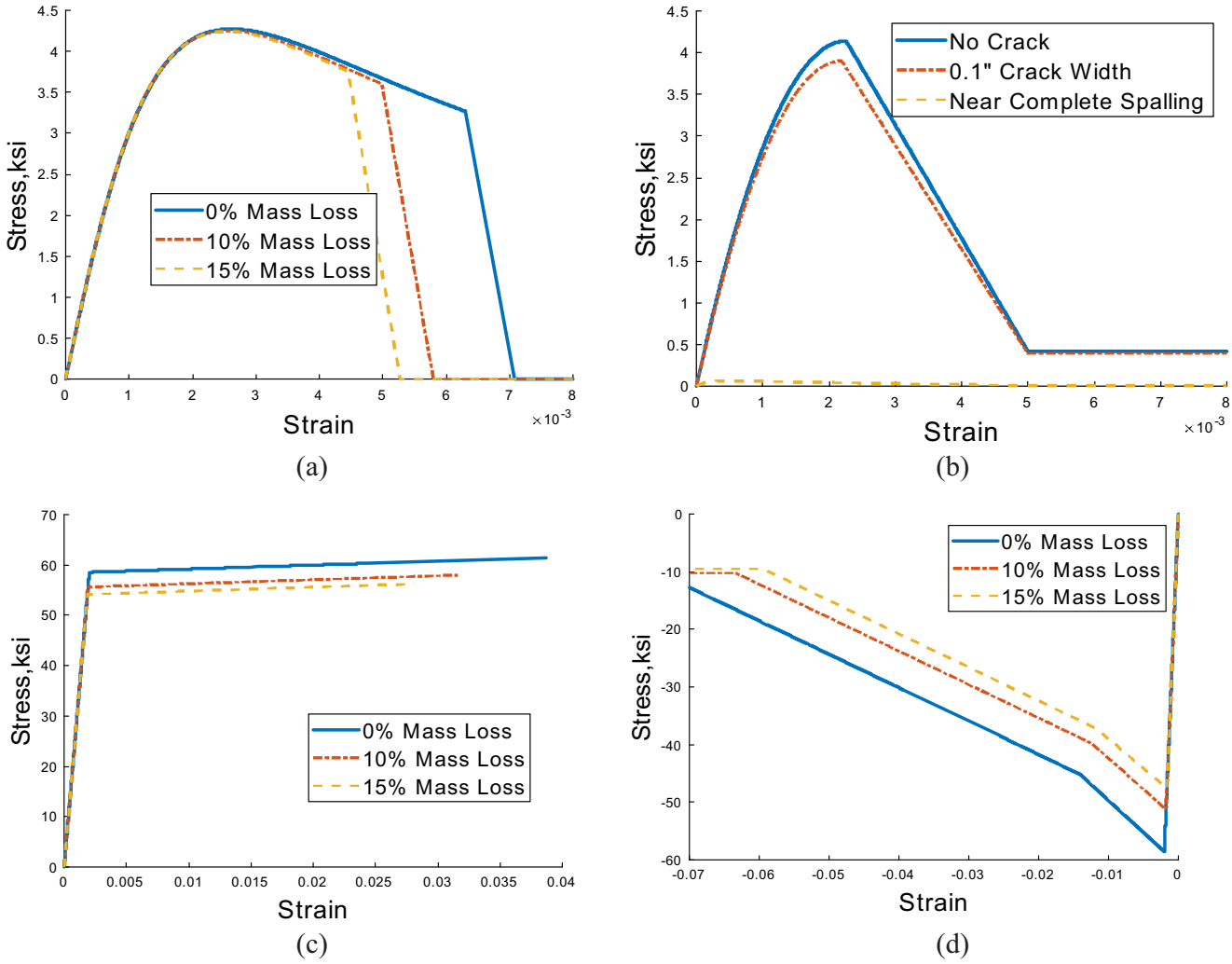


**Fig. 3.** Material stress–strain behavior with effect of corrosion and cracking for (a) core concrete, (b) cover concrete, (c) steel in tension and (d) steel in compression with bar buckling.

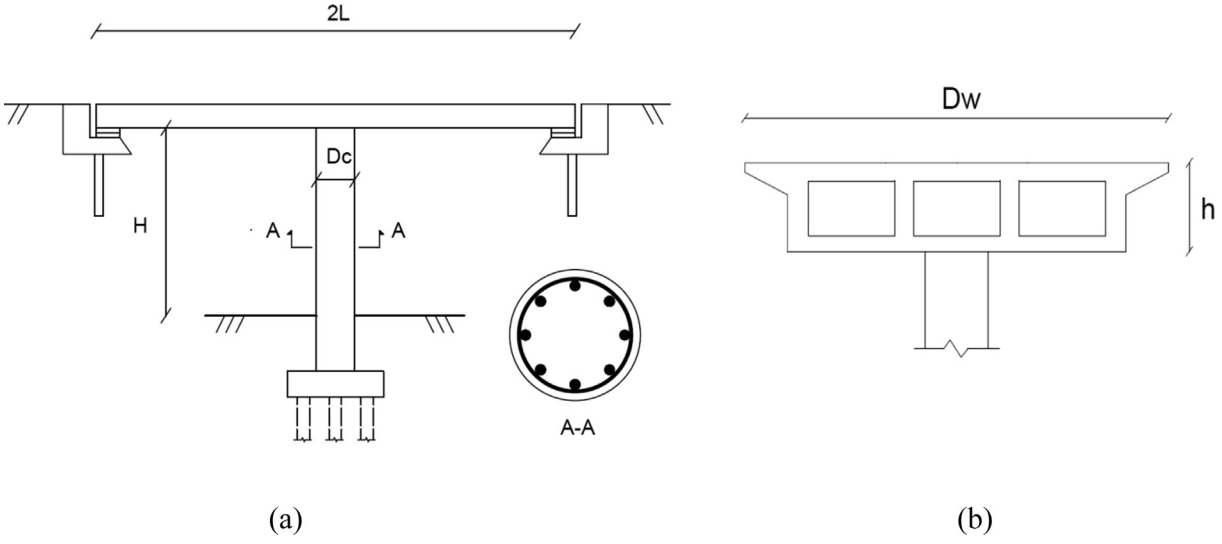


**Fig. 4.** (a) Longitudinal view and (b) transverse view of sample bridge.

resistance considers the resistance contributed by the piles alone. This study uses 'HyperbolicGapMaterial' in OpenSees to simulate the backfill response, and the backfill model is based on the work proposed by Shamsabadi and Yan [53]. The abutment pile provides both transverse and longitudinal resistance at the abutment. This study uses the 'Hysteretic' material with a zero-length spring to

**Table 1a**
Mean and variance values of geometric parameters of the sample bridges.

| Geometric Parameters | Distribution Type | Mean | Variance |
|---|---|---|---|
| Span length (L) | Lognormal | 32.3 m | 77.9 $m^2$ |
| Deck width (Dw) | Lognormal | 10.4 m | 2.8 $m^2$ |
| Column height (H) | Lognormal | 6.5 m | 0.60 $m^2$ |
| Depth of bridge deck (h) | Lognormal | 1.8 m | 0.24 $m^2$ |

**Table 1b**
Distribution details for mechanical and material parameters of the sample bridges.

| Mechanical Parameters | Distribution Type | Distribution Parameter 1 | Distribution Parameter 2 |
|---|---|---|---|
| Concrete compressive strength | Normal | 34.5 MPa (mean) | 4.3 MPa (standard deviation) |
| Yield strength of steel | Lognormal | 460 MPa (mean) | 0.08 (coefficient of variation) |
| Shear modulus of elastomeric bearing pad | Uniform | 551.6 MPa (lower bound) | 1723.7 MPa (upper bound) |
| Longitudinal reinforced ratio of column | Uniform | 1.0 % (lower bound) | 3.5 % (upper bound) |
| Transverse reinforced ratio of column | Uniform | 0.4 % (lower bound) | 1.7 % (upper bound) |
| Damping ratio | Normal | 0.045 (mean) | 0.0125 (standard deviation) |

model the pile response based on the trilinear model recommended by Choi [13]. Following the recommendations by Nielson [45], Padgett [48], and Ramanathan [50], the damping is modeled assuming a normal distribution. Moreover, the study uses 0.02 and 0.07 for the 2nd and 98th percentile of the bridge damping ratio, respectively [8], resulting in a normal distribution with a mean of 0.045 and a standard deviation of 0.0125 that is adopted herein. For the highway bridges' fragility assessment, the study mainly focuses on the damage that occurs in the bridge column with displacement ductility as the engineering demand parameter. The damage states used to quantify the levels of the damage are shown in Table 2 with flexural dominant failure mode. A suite of ground motions is selected from the NGA-2 database [11], consisting of 160 motions matching California's hazard characteristics for which this bridge type is common. Fig. 6 shows the response spectra of the ground motions in the two horizontal directions.

## 6. Results

This work aims to update the original fragility curve with new observational data to obtain the new fragility function with reduced computational cost. Therefore, it is assumed that the original fragility function is known from prior analyses. The original fragility curve need not be obtained from running nonlinear time history analyses on a full structural finite-element model, but it can also be from the literature, expertise, or empirical data. The updating is done by taking limited observational data to calculate fragilities using the derived Bayesian updating rules, rather than running the full set of nonlinear time history analyses with a sufficient number of ground motions to obtain stable fragility function parameters.

In this case, new data is taken as observations of the response under corrosion conditions in the column. Therefore, the original fragility function refers to the fragility curve with a pristine bridge column, and the updated fragility function provides the fragility with a corroded bridge column. The following section presents results from using two types of numerical data to update the fragility function. The first type of data refers to the bridge column's displacement ductility under seismic loadings from analyzing the full-bridge response, i.e., using the full structural finite-element

**Table 2**
Description of damage states.

| Flexure-Critical Column | Description | Damage Level |
|---|---|---|
| DS-1 | Significant Cracking | Slight |
| DS-2 | Initial Spalling | Moderate |
| DS-3 | Core Exposure | Extensive |
| DS-4 | 20% Strength Degradation | Complete |

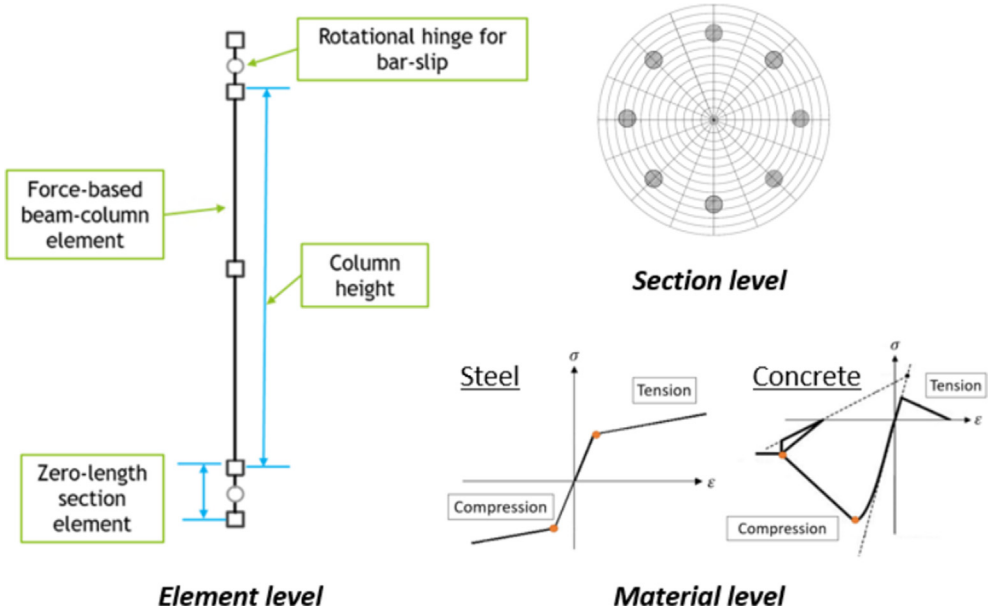


**Fig. 5.** Numerical model for bridge column.

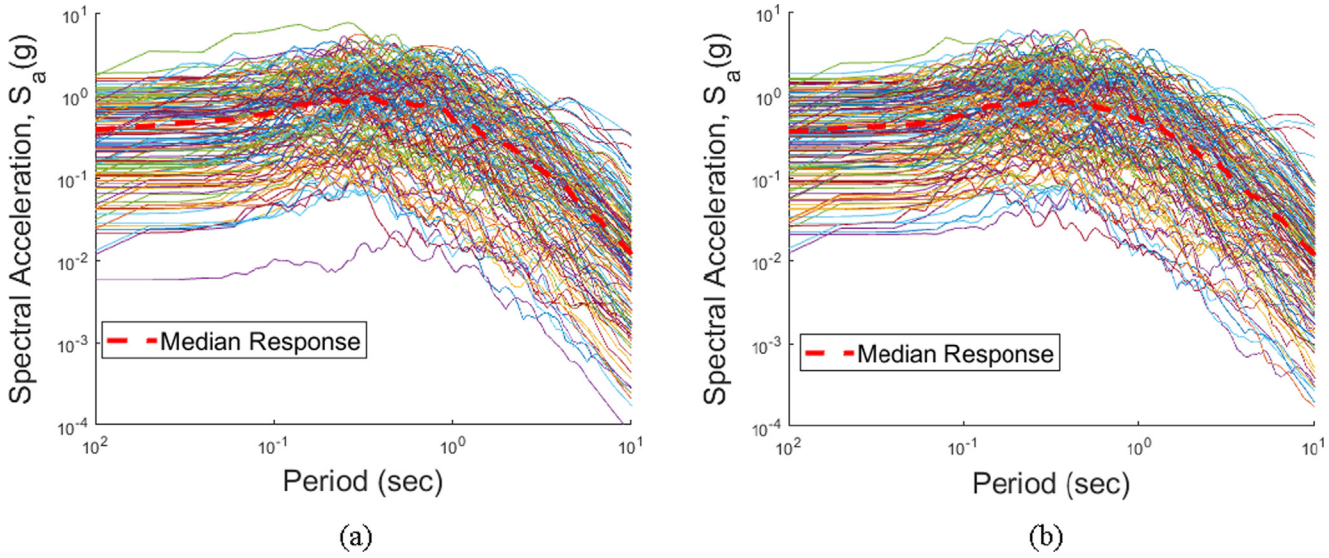


**Fig. 6.** Response spectra for the selected ground motions in (a) horizontal component one and (b) horizontal component two.

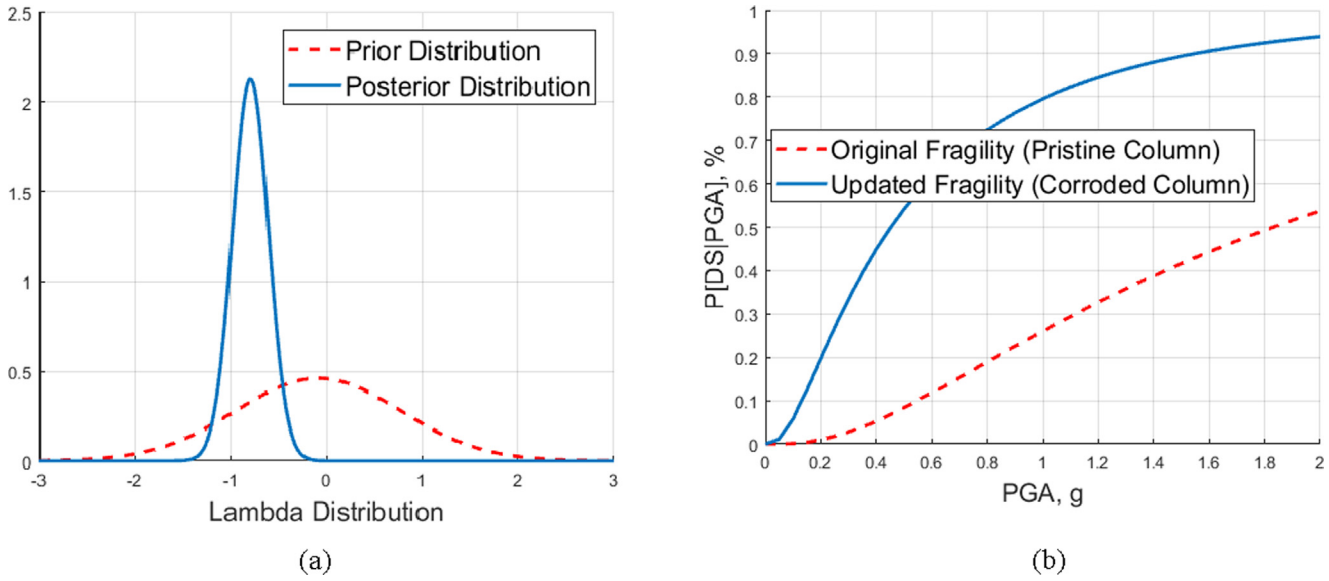


**Fig. 7.** (a) Prior distribution compared to posterior distribution for $\lambda_m^{'}$ and (b) original fragility curve (pristine column) for collapse damage state compared to updated fragility curve (corrosion with 20% mass loss of reinforcement) using 25 observational data points.

model; the second type of data refers to the displacement ductility of the bridge column under seismic loadings considering the single column only. The resulting performance of the proposed approach in terms of accuracy and computational cost are compared with existing methods for both types of observational information.

### *6.1. Bayesian updating of fragility curves considering full bridge model*

The results in this section use observational data computed from the bridge column's displacement ductility based on nonlinear time history analyses considering the response of the entire bridge under a particular corrosion level. As is typical for fragility assessments, the full structural finite-element model is required. However, the number of dynamic analyses required using the proposed method compared to the existing method to obtain stable fragility results differs. To show the impact of corrosion on structural performance, Fig. 7(a) shows the prior and posterior distributions of the unknown parameter $\lambda_m^{'}$ with 25 observational data points. Fig. 7(b) shows the original and updated fragility curves for the collapse damage state using these 25 observational data points. The original fragility curve represents fragility for the pristine bridge column; the updated fragility curve represents fragility with a corroded column with a 20% mass loss of reinforcement. Mass loss of reinforcement is used as a measure of corrosion as a readily obtainable structural inspection parameter [31].

To assess the proposed approach's accuracy, Fig. 8 shows the fragility results across the four damage states from using the proposed approach compared with the exact result. The exact result is taken as the fragility function generated by running nonlinear time history analyses over the full set of 160 ground motions. The updated fragility curves for each damage state are shown, including 95% confidence bounds from the proposed approach computed using 25 and 50 observational data points, compared to the exact fragility curve.

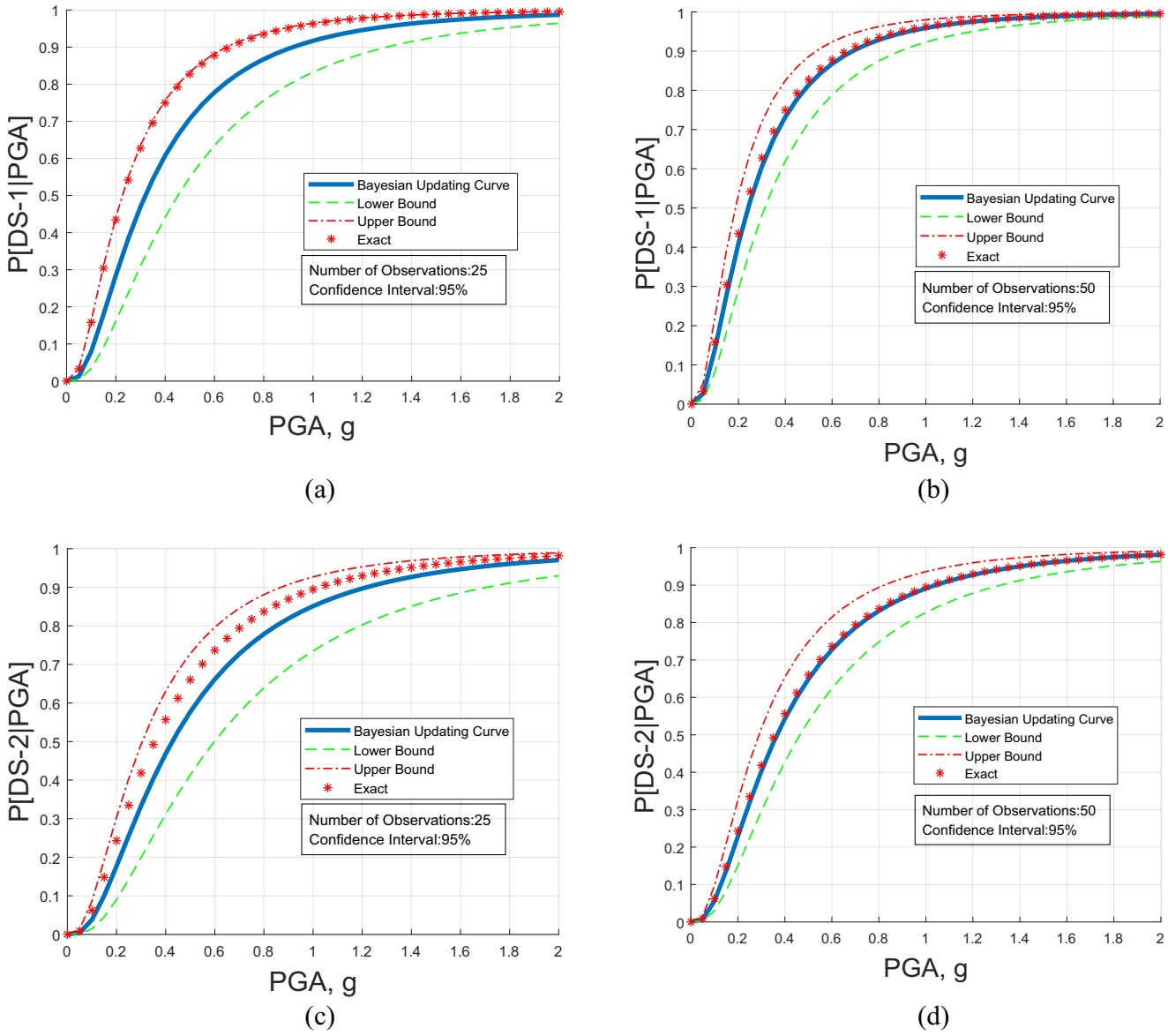


**Fig. 8.** Bayesian updated fragility curve compared to exact fragility curve considering 25 observational data points (left) and 50 observational data points (right) for (a) & (b) DS-1, (c) & (d) DS-2, (e) & (f) DS-3, and (g) & (h) DS-4.

In Fig. 8, the narrowing of the confidence bounds in using 50 compared to 25 observational data points is observed. As expected, more accurate results using the Bayesian updating approach are obtained as the number of observational data points increases. The maximum failure probability differences between the results from the Bayesian updating approach using 25 and 50 observational data points and the exact result are 16% and 2% for DS-1, 9% and 2% for DS-2, 12% and 8% for DS-3, and 9% and 4% for DS-4, respectively. The exact result lies within the 95% confidence bounds in both cases and for all damage states.

To further quantify the proposed method's performance and assess differences in achieving convergence between the proposed and existing approaches, a comparison of the performance as the number of observations increases is also investigated. Fig. 9(a) and 9(c) show the evolution of the lognormal mean and variance as the number of observations increases for both approaches. Note that the existing approach employs the standard method of moments to estimate the fragility parameters, and the ordered set of ground motions is used to limit the influence of randomness in loading intensities on the variability of the results for the existing method. Fig. 9(b) and (d) show the error of the lognormal mean and variance from the exact value as the number of observations increases for the two approaches.

Fig. 9 shows that the lognormal mean converges faster and more smoothly using the proposed Bayesian updating method compared with the existing approach. In the existing approach, the parameters for the fragility function are generated based on PSDMs. The Bayesian updating approach evaluates the lognormal parameters by updating rules and calculating the mean as in Eq. (14a), resulting in smoother estimates of the parameters. The smoothness in the convergence of parameters is even more apparent in the convergence of the variance. The maximum error of the lognormal mean is 50% for the proposed compared with 260% for the existing approach, while the maximum error of the variance is 21% for the proposed compared with 490% for the existing approach. The sudden increases in error that occur for both the lognormal mean and variance in Fig. 9, particularly for the existing method, are due to the consideration of outliers from the numerical results. This outcome shows the instability of the existing approach in the presence of outliers. In contrast, the proposed

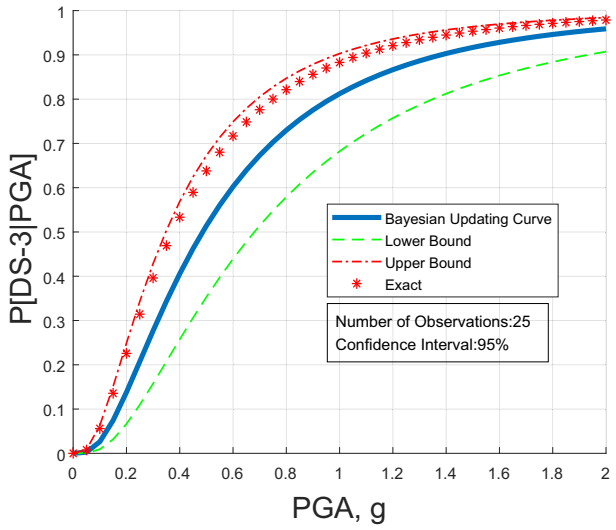


(e)

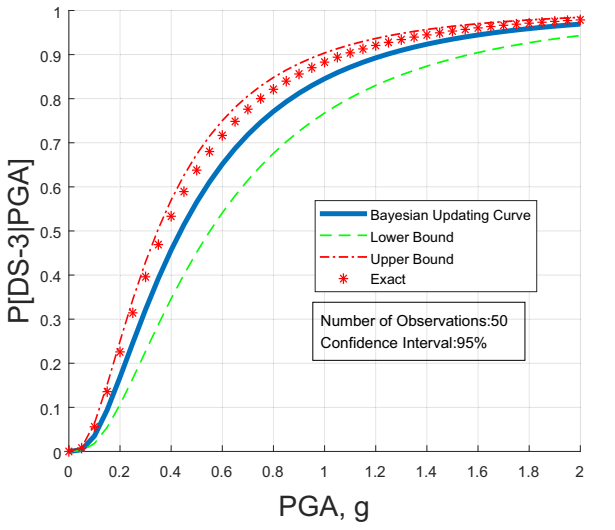


(f)

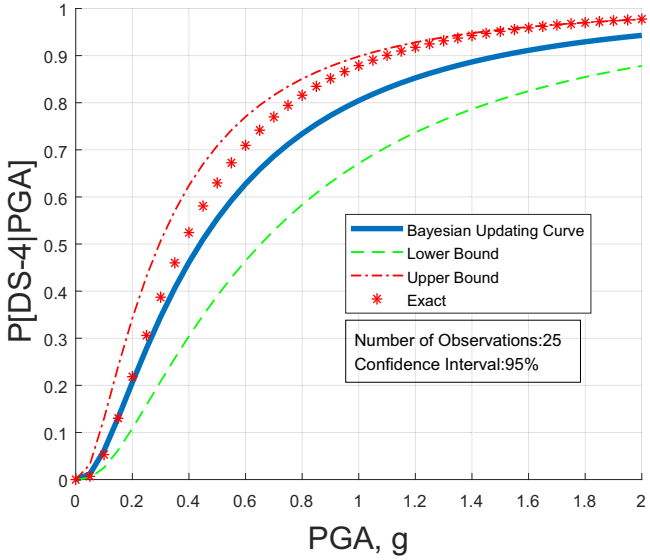


(g)

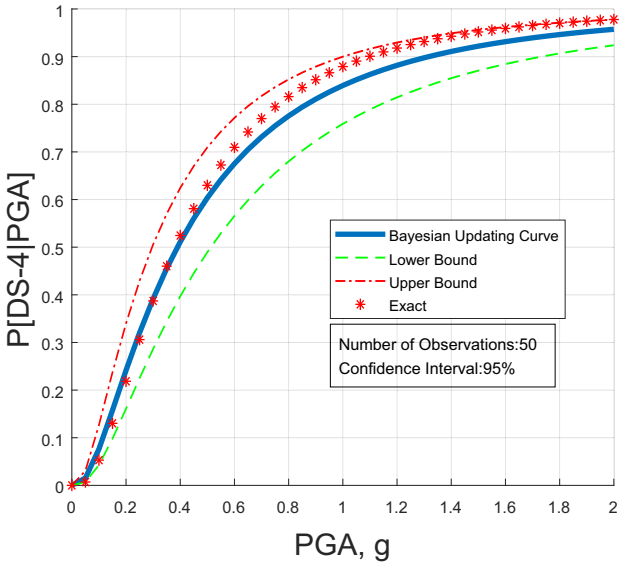


(h)

**Fig. 8** (*continued*)

approach provides more reliable results, predicting the variable values in a more stable and consistent manner.

Fig. 10 investigates the accuracy of the two approaches, showing the errors in terms of the root mean square error (RMSE) for the fragility curves over the full range of PGA values, as well as the maximum differences in probabilities of exceeding each damage state for the proposed compared to existing approaches. The study utilizes the results from running analyses over the full set of 160 ground motions as the benchmark results for comparison. The percentage errors obtained from both the proposed and existing approaches are calculated in comparison with the benchmark points as a function of the number of observational data. Fig. 10 shows RMSE and the maximum difference in failure probability for probabilities of exceeding damage states DS-1 through DS-4. The plots for the existing approach begin at seven data points because the first six data points generate a negative slope in the PSDM (i.e., a negative $b_m$ value in Eq. (5b)), which consequently leads to a negative lognormal variance from Eq. (6c).

From Fig. 10, the proposed Bayesian updating approach leads to a smoother result with faster convergence and lower error compared to the existing approach. In all cases, the proposed approach converges to a lower RMSE and lower maximum probability difference than existing methods, indicating increased accuracy of the proposed approach. To facilitate comparison between the two approaches, a threshold of 6% and 10% are chosen for RMSE and maximum probability difference, respectively, based on the convergence values of the results. The proposed approach achieves faster convergence to these accuracy threshold values and more stable results. For example, looking at the most extreme damage state DS-4, the proposed approach requires only 25 observational data points to reduce RMSE and the maximum difference in failure probability to below 6% and 10%, respectively. In addition, once a minimal RMSE and maximum probability difference level is achieved, the outcome remains stable using the proposed approach. In comparison, it requires more than 50 observational data points for existing methods to reach the minimum RMSE

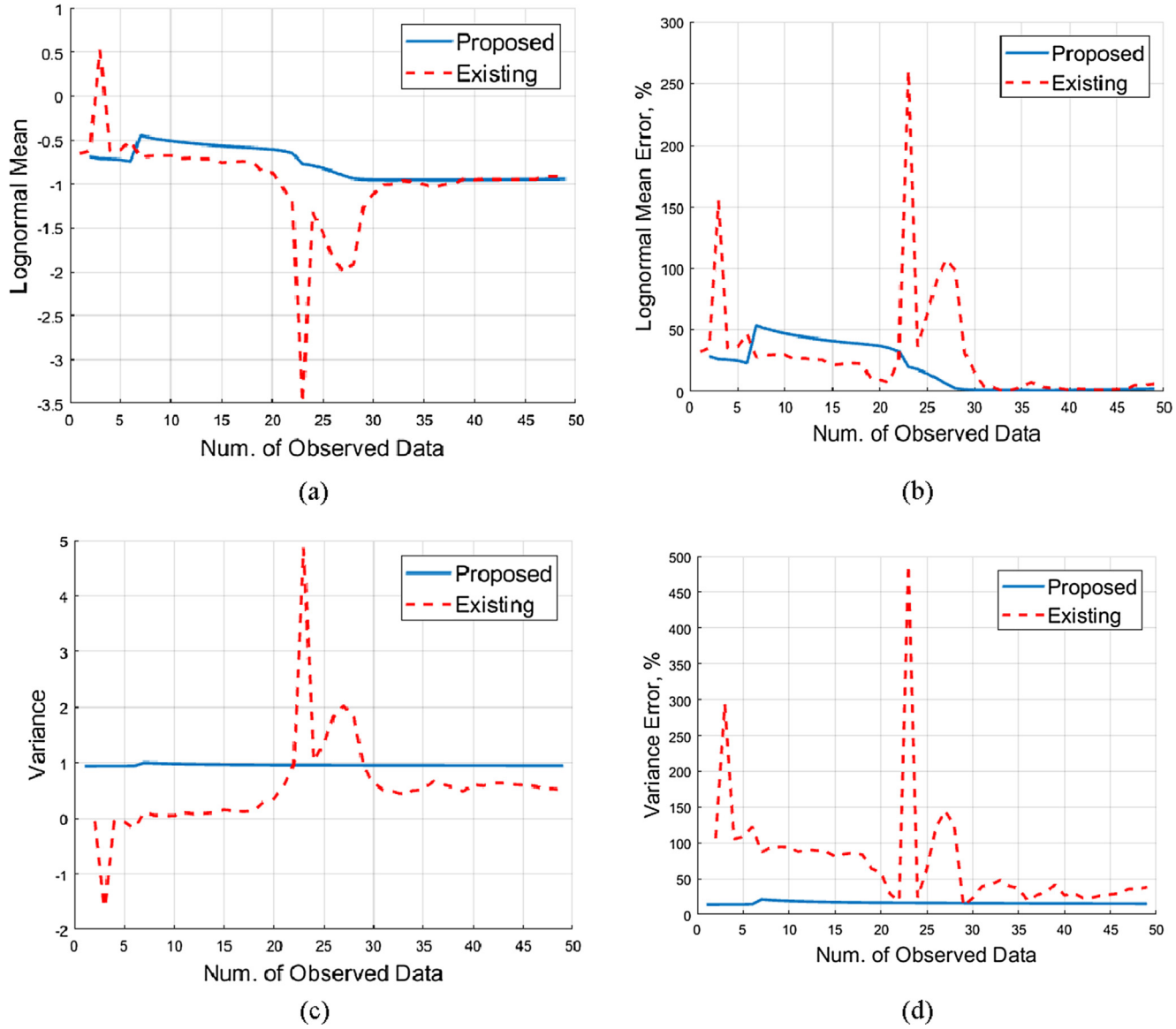


**Fig. 9.** (a) Evolution and (b) error of lognormal mean, and (c) evolution and (d) error of variance between the exact value and results from the proposed and existing approaches for DS-4 under 20% mass loss.

and probability difference thresholds. The instability of results using the existing approach is also seen as the RMSE, and probability difference values are observed to increase. These trends in terms of accuracy, convergence, and stability are observed for the other damage states as well.

The proposed approach gives a relatively better prediction for DS-1 and DS-2 compared with DS-3 and DS-4, particularly when 50 observational data points are used as shown in Fig. 8, because the lower damage state datasets exhibit less variability than the higher damage datasets. However, from the results in Fig. 10, it is shown that the proposed approach not only renders smaller values in terms of RMSE and maximum difference with fewer numbers observed data required than that for the existing approach for DS-1 to DS-4, but it also gives a more stable prediction once a specific number of observed data is provided in comparison with the existing approach. Table 3 summarizes the number of analyses required to reduce RMSE and maximum difference to below the 6% and 10% thresholds, respectively, as well as the minimum RMSE and probability difference achieved for each damage state.

From Table 3, for all damage states, existing approaches require an average of 64 and 79 analyses for the RMSE and maximum probability difference to reduce below 6% and 10%, respectively. Comparatively, it takes an average of 25 analyses for the proposed approach to do so. The average computational time saved to obtain updated fragility functions for each damage state is more than 60%, with a savings of 61% to achieve RMSE under 6% and a savings of 68% to achieve a maximum probability difference under 10%. To evaluate the accuracy of the approaches, the minimum RMSE and minimum probability difference achieved are compared. As existing methods show unstable results, the minimum error values achieved over 50 observational data points for both approaches are shown to facilitate consistency in the comparison. The proposed approach achieves more accurate results (lower RMSE and lower probability difference) across all damage states, except for DS-3 which the values are close. The results show that the proposed approach is able to achieve accurate and stable updated fragility assessments with fewer data points and significantly reduced computational cost compared to existing methods.

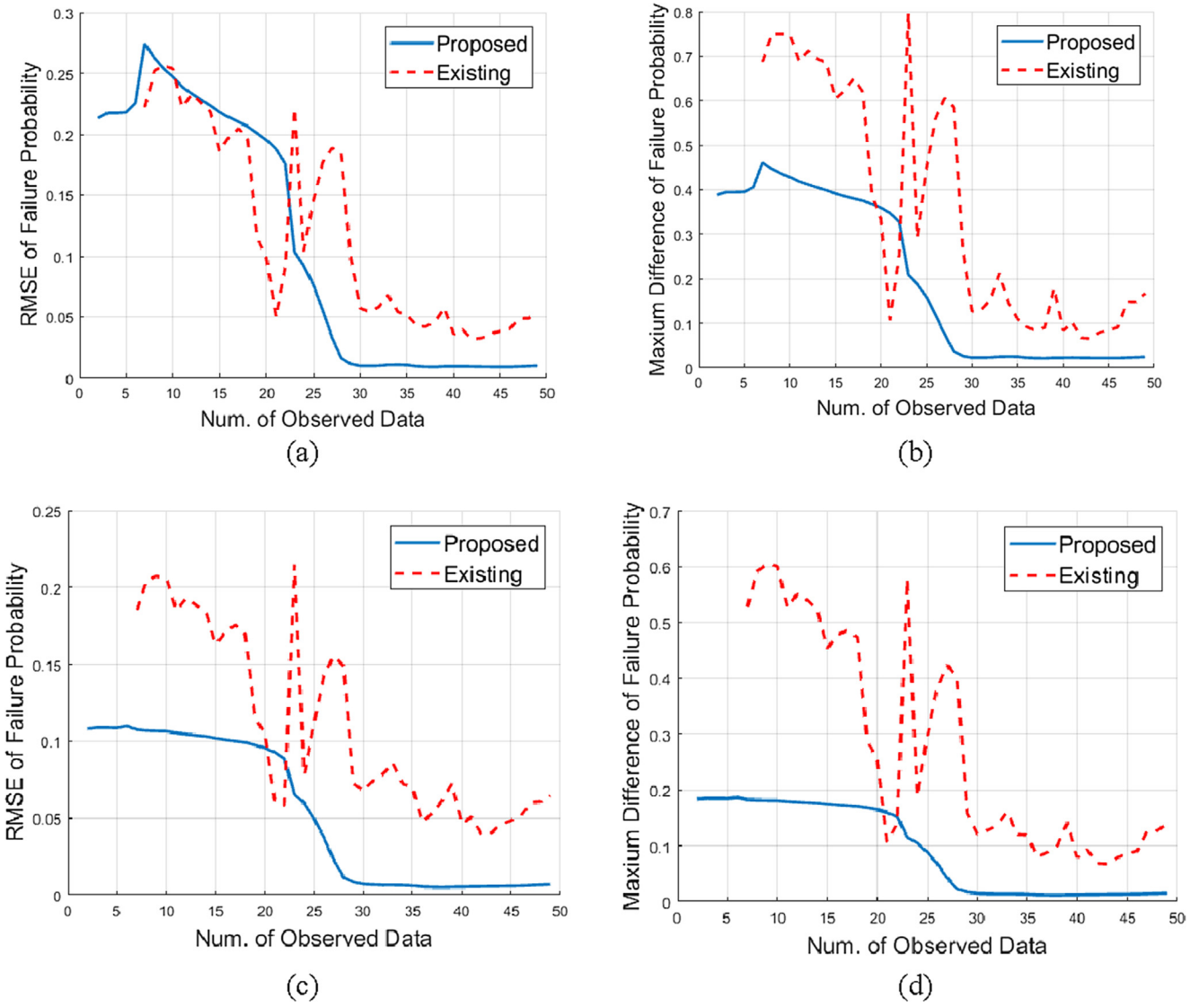


**Fig. 10.** RMSE and maximum difference of failure probability for (a) & (b) DS-1, (c) & (d) DS-2, (e) & (f) DS-3, and (g) & (h) DS-4 for the proposed compared to existing approaches considering full bridge response.

### *6.2. Bayesian updating of fragility curves considering single column only*

Results in the previous section show the reduction in the number of analyses possible using the proposed method. However, a full structural finite-element model is required. This section investigates the further reduction of computational cost by using information from a reduced complexity finite-element model. Instead of performing nonlinear time history analyses at the full-bridge level, this section considers data from nonlinear time history analyses performed on the column level only with the same set of ground motions that was used for the full bridge response. The bridge column is modeled based on Fig. 5 for this component-level study, and the same amount of axial load from the superstructure is imposed at the top of the column. The bond-slip effect has been considered by applying a zero-length bond-slip element at the end of the beam-column model. More details can be found in the prior section describing the bridge modeling. The goal here is to investigate the ability to use component-level analyses to update estimates of full structural performance. If possible, the time to obtain the updated fragility functions can be further reduced by decreasing the degrees of freedom and complexity of the structural model and analyses. The reduced component-level models can be applied to the critical structural component with maximum damage accumulation, and this requires either engineering judgment or understanding of the structural response at the system level. Another way to figure out the critical location is to conduct a static/dynamic analysis to identify the component with the dominating structural response as such components will typically govern the structural response under a particular loading situation, and would thus be selected for the reduced component-level modeling.

For the case of the bridge structure, the column behavior often dictates the bridge behavior. Therefore, the reduced finite-element model is taken to be a single column only. The following results show the use of the proposed Bayesian updating approach performed based on the outcomes of nonlinear analyses of the single column to obtain updated fragility curves considering the effect of measured corrosion.

As structural analyses of the column only are significantly less computationally intensive compared to the full-bridge structure, 51 nonlinear time history analyses are performed on the bridge

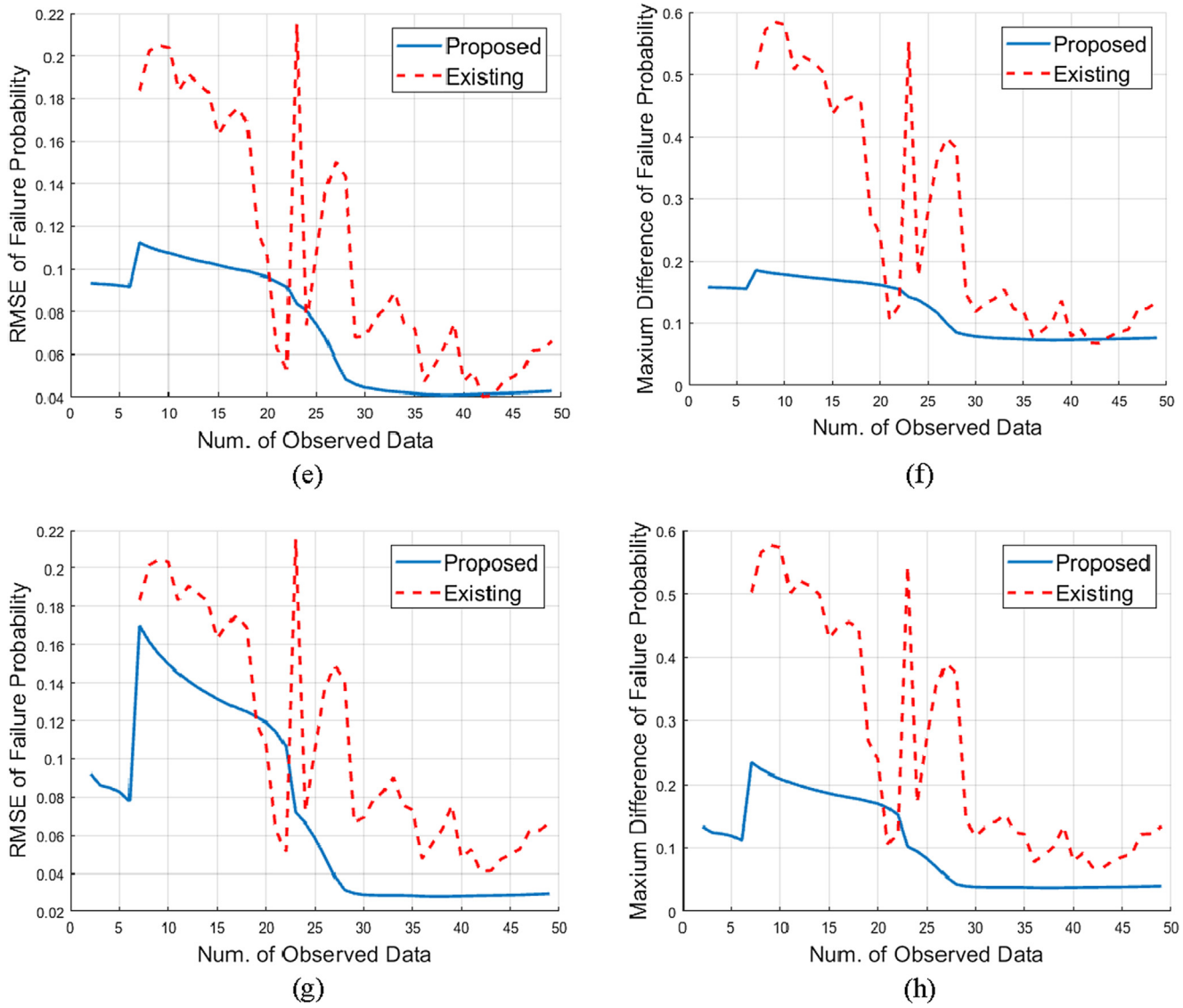


**Fig. 10** (*continued*)

**Table 3**
Comparison of computational cost and accuracy between the proposed (full-bridge response) and existing approaches.

| Num. of Analyses Required | RMSE $\leq$ 6% | | Max. Prob. Diff. ($\leq$10%) | | Min. RMSE (%) with 50 Observed Data | | Min. Max. Prob. Diff. (%) with 50 Observed Data | |
|---|---|---|---|---|---|---|---|---|
| | Proposed | Existing | Proposed | Existing | Proposed | Existing | Proposed | Existing |
| DS-1 | 26 | 61 | 26 | 80 | 0.87 | 3.20 | 2.12 | 6.51 |
| DS-2 | 25 | 65 | 25 | 79 | 0.50 | 3.96 | 1.11 | 6.71 |
| DS-3 | 26 | 65 | 26 | 79 | 4.07 | 4.02 | 7.29 | 6.77 |
| DS-4 | 25 | 65 | 23 | 79 | 2.78 | 4.07 | 3.74 | 6.85 |

column, which are transformed to 50 observational data points. The computational requirements for conducting these analyses are provided at the end of this section. The procedures shown in Fig. 2 are then applied to the single-column responses to obtain updated fragility curves of a corroded bridge column. It is noted that the prior distribution for this data type is also computed based on single-column analyses rather than the full-bridge response. To show how the proposed method performs as the expected performance of the structure varies, e.g., with varying levels of corrosion, Fig. 11 shows the resulting fragility curves considering 10% mass loss of reinforcement (left-hand plots) and 20% mass loss (right-hand plots) for each of the four damage states. The results from the proposed method, including 99% confidence bounds, are shown compared to the exact value obtained from running the full set of 160 nonlinear time history analyses on the full bridge finite-element model.

From Fig. 11, the Bayesian updating approach is able to predict the fragility parameters and accurately update the fragility functions based on the limited data obtained from the reduced finite-element model of the displacement ductility between the pristine and corroded column. The exact value lies within the 99% confidence bounds in all cases except for DS-4 at low PGA values. In

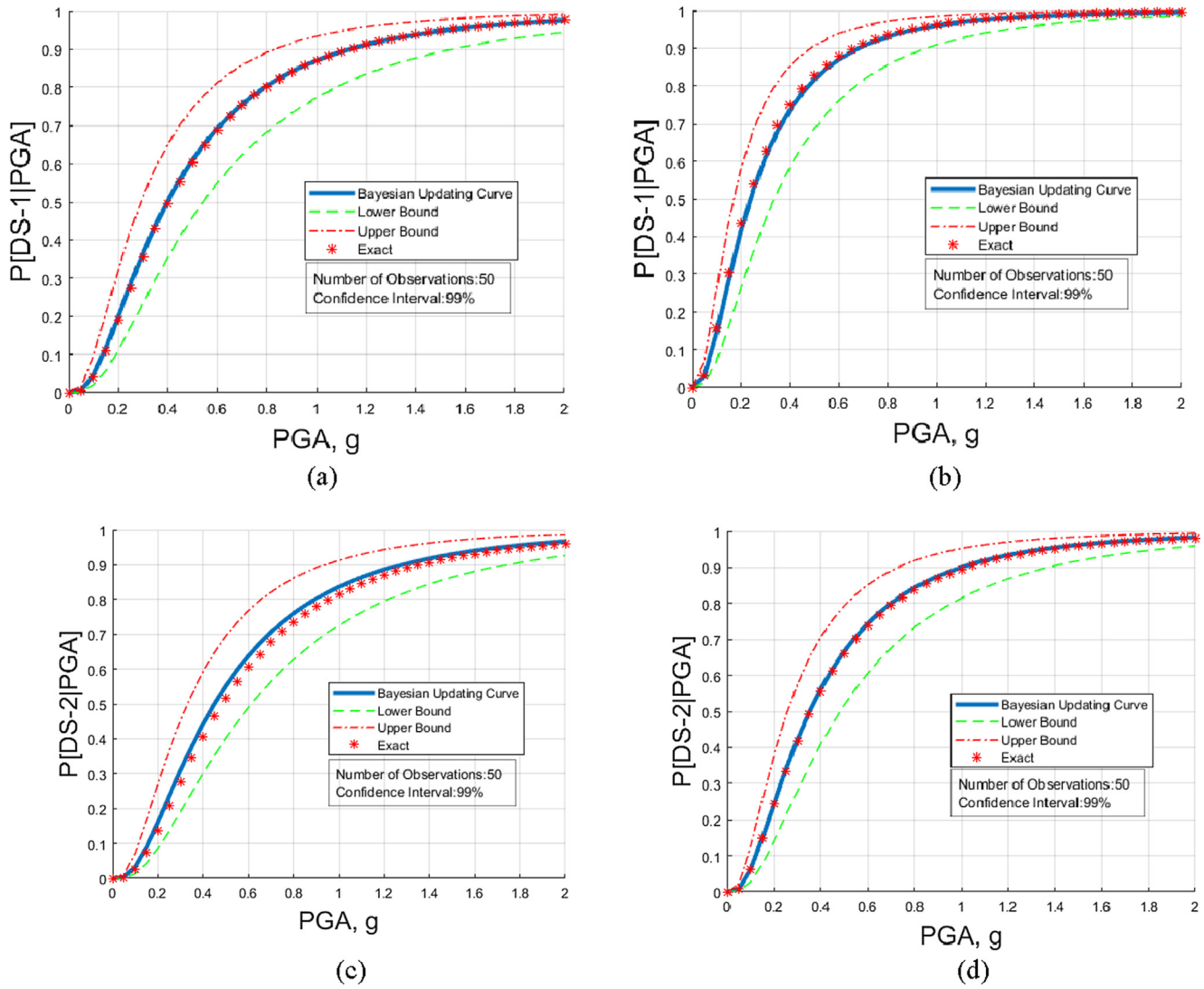


**Fig. 11.** Bayesian updated fragility curve compared to exact fragility curve considering 10% mass loss of reinforcement (left) and 20% mass loss (right) for (a) & (b) DS-1, (c) & (d) DS-2, (e) & (f) DS-3, and (g) & (h) DS-4.

Fig. 11, as expected, there is a certain level of difference between the Bayesian updated result and the exact result due to the simplification of the dataset. The observational data is generated from a single column time history analysis under a particular corrosion level and does not include constraints from the superstructure that may affect the column's response. However, the error is small compared to the time saved to obtain the fragility function. This is due to not needing to build the full bridge model, as well as faster runtimes for each analysis with a reduced complexity structural model. Similar to Fig. 8 for the full-bridge response results, Fig. 12 shows the RMSE and maximum probability difference between the proposed approach and the existing approach considering the single column response. For all damage states, the proposed method shows faster convergence to lower error results than the existing method. Table 4 quantifies the difference. Taking the RMSE and maximum difference thresholds again as 6% and 10%, respectively, the average number of analyses required to move below these error thresholds is 24, compared to averages of 64 and 79 for the existing method, respectively. Furthermore, the computational time required for each of these simplified-column analyses is significantly reduced compared to the existing approach based on results from the full-bridge model. Table 4 shows that the minimum RMSE and probability difference achieved is significantly lower, resulting in more accurate results using the proposed approach for each damage state. The outcomes show that even with data from the reduced complexity finite-element model, the proposed approach results in faster convergence and increased accuracy compared to existing approaches.

Table 5 summarizes the computational cost of running nonlinear time history analyses for the full-bridge model compared to a single column for the exact, existing, and proposed approaches. As shown in Figs. 8 and 9 and Tables 3 and 4, as the number of analyses required to obtain stable fragilities varies somewhat across the damage states, where applicable, the average number of analyses required for the four damage states is shown. All analyses are conducted on a computer with 16.0 GB RAM and i7-3770 processor. Note that readers can follow the proposed flowchart (Fig. 2) to complete the updating procedure using the derived equations, which can be easily set up in advance. The updating process itself does not require any processing time as it follows the derived updating rules. It can be performed either simultaneously with the finite-element simulations or used as a post-processing tool to analyze simulation results.

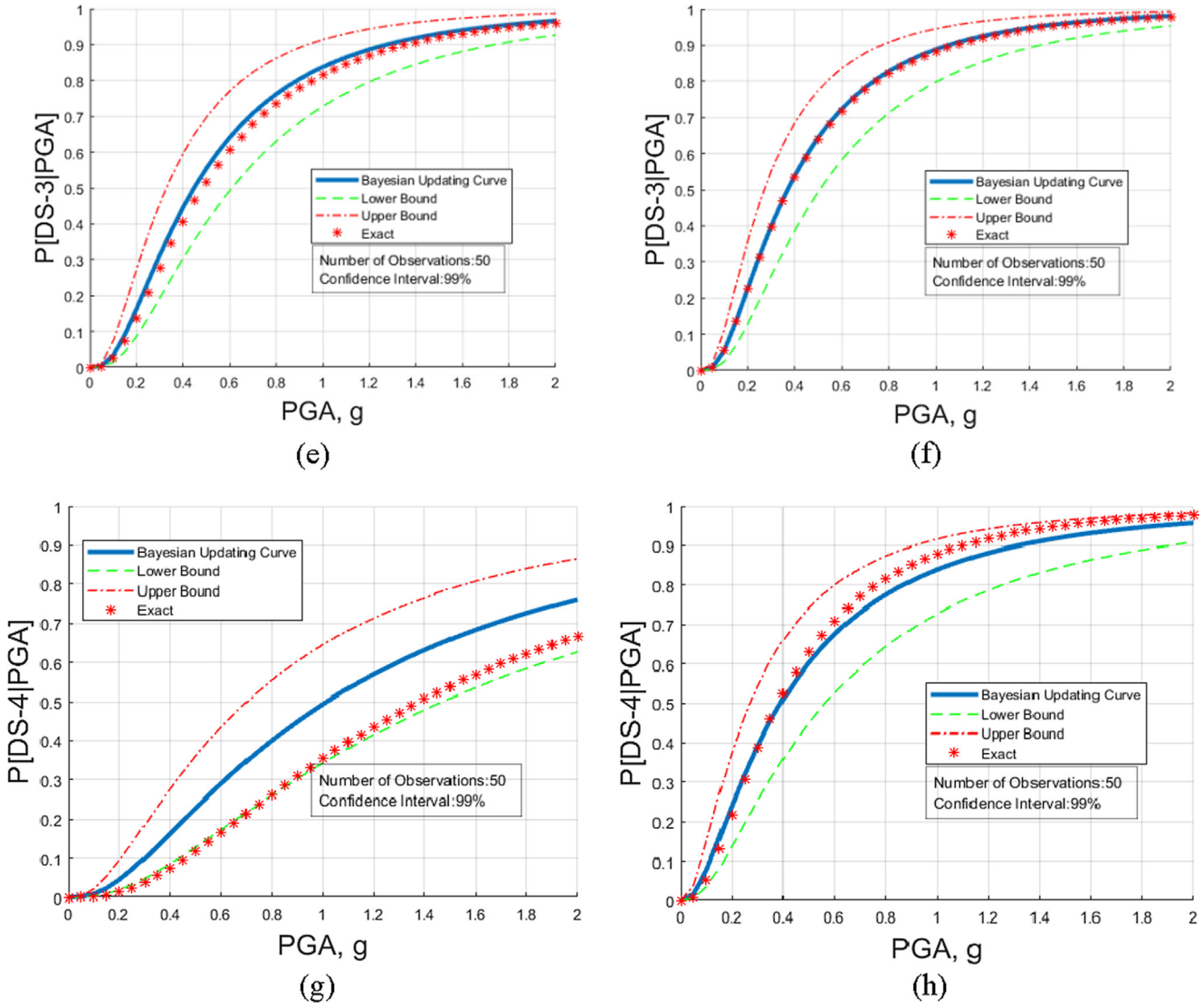


**Fig. 11** (*continued*)

Table 5 considers only the single-column model combined with the proposed Bayesian updating approach, significantly reducing the computation cost, with more than an order of magnitude savings from existing methods. Comparing with each method, the computation time needed to obtain a stable updated fragility curve for the corroded states is reduced by 98.7%, 96.8%, and 91.4% compared to the exact, existing, and proposed approaches considering the full bridge model, respectively. The savings in a computational effort to build just a single column model compared to the full finite-element bridge model is significant in addition to the analysis time. Combining the reduced observational data type with the proposed Bayesian updating approach achieves updated fragility assessments with sufficient accuracy in failure probability from the target fragility function for all damage states across hazard intensities.

## 7. Conclusions

Dynamic analysis of large and complex finite-element models is typically accompanied by high computational costs, especially for high-fidelity structural finite-element models. Running probabilistic analyses with a series of nonlinear dynamic analyses for problems considering a range of uncertainties requires even more computational effort to obtain stable results, including to construct fragility functions assessing structural risk. This paper presents a methodology to obtain updated analytical fragility curves through a Bayesian updating approach that is able to achieve accurate and stable results with significantly decreased computational cost. The conjugate Bayesian approach reduces the computational cost associated with numerical integration. Instead, it directly modifies the prior distribution parameters through updating rules to obtain a closed-form expression for the posterior. The study uses observational data points generated based on the nonlinear time history response (i.e., displacement ductility of the bridge column under a particular corrosion level) from the numerical model to update the fragility. The selection of the data points for updating consists of two main parts. First, the ground motions used for generating numerical observational data are selected, in this case from the NGA-2 database consisting of 160 motions matching the hazard characteristics for which the studied bridge type is common. Second, the sequence of the ground motions used for the nonlinear time history analysis is ordered such that the numerical data points start at the mean PGA value and oscillate around the mean

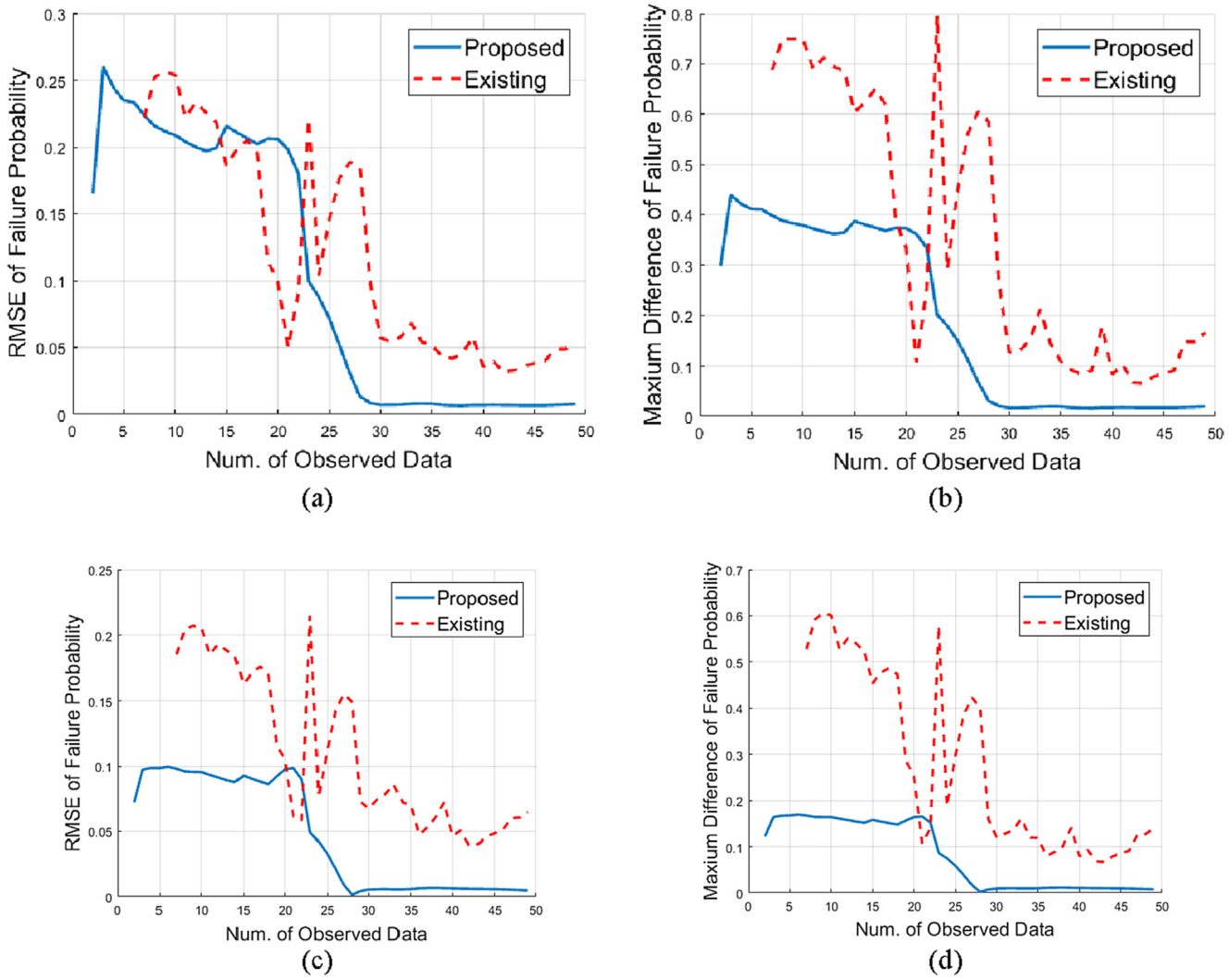


**Fig. 12.** RMSE and maximum difference of failure probability for (a) & (b) DS-1, (c) & (d) DS-2, (e) & (f) DS-3, and (g) & (h) DS-4 for the proposed compared to existing approaches considering single column response.

with increasing deviation from the mean. This reduces the randomness in the outcome and improves the robustness of the proposed framework. The methodology is applied to assess the fragilities of bridges considering the effect of corrosion.

Using the proposed updating rules in the context of conjugate Bayesian inference, the proposed method decreases the time to obtain stable fragility functions by reducing the number of nonlinear time history analyses required. The proposed approach shows faster convergence and results in more stable estimates of the fragility function parameters. Compared to existing methods, the proposed approach reduces the computational cost by 61% to achieve RMSE under 6% and by 68% to achieve maximum probability difference under 10%. It is proposed to reduce computation time even further by performing nonlinear analyses at the component level only rather than for the full structure. Doing so reduces the computational cost by as much as 96.8% compared to existing approaches, with the 95% confidence interval fragility estimates capturing the exact fragility values across almost all damage states and loading intensities. While the proposed approach is demonstrated to update the fragility function based on numerical structural response information considering the effect of measured corrosion levels, the proposed approach provides a framework that enables updating fragility curves by combining information from experimental testing and hybrid simulation, or other types of observational data (i.e., sensor data, etc.).

As structures age, the safety evaluation and risk assessment of aging structures under natural deterioration mechanisms (e.g., corrosion attack) and dynamic loading conditions (e.g., seismic hazards) is becoming increasingly critical. A faster and more reliable method is needed to accomplish this goal. The proposed method provides researchers and engineers with an efficient, accurate, and reliable approach to perform bridge risk assessments. It provides a tool to perform seismic fragility assessment of aging structures with ease, facilitating engineering tasks such as identifying the most vulnerable bridges in a network, and prioritizing resources for rehabilitation, retrofit, and repair to protect critical assets. In addition, in light of recent developments [19,51,6], one could incorporate the proposed approach to evaluate and assess the resilience of structures in conjunction with models such as digital twins for efficient updating of structural analysis results considering factors such as multiple natural hazards and climate change.

**Appendix**: Comparison of performance between normal and lognormal prior distributions.

The following comparison is performed in terms of resulting RMSE and maximum difference of failure probability for DS-4 with

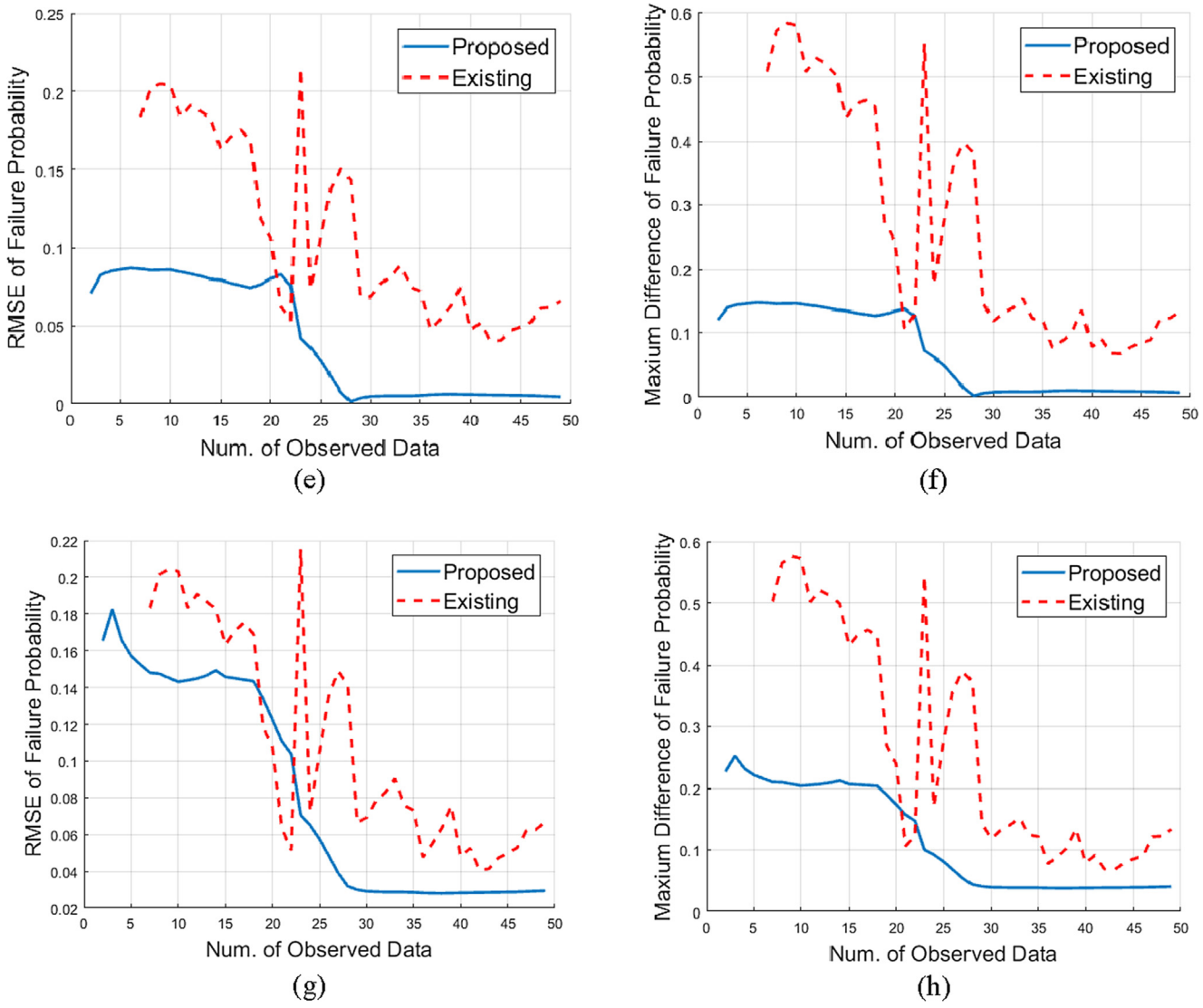


**Fig. 12** (*continued*)

**Table 4**
Comparison of computational cost and accuracy between the proposed (single column response) and existing approaches.

| Num. of Analyses Required | RMSE $\leq$ 6% | | Max. Prob. Diff. ($\leq$10%) | | Min. RMSE (%) with 50 Observ. Data | | Min. Max. Prob. Diff. (%) with 50 Observ. Data | |
|---|---|---|---|---|---|---|---|---|
| | Proposed | Existing | Proposed | Existing | Proposed | Existing | Proposed | Existing |
| DS-1 | 25 | 61 | 26 | 80 | 0.65 | 3.20 | 1.63 | 6.51 |
| DS-2 | 23 | 65 | 23 | 79 | 0.14 | 3.96 | 0.22 | 6.71 |
| DS-3 | 23 | 65 | 23 | 79 | 0.15 | 4.02 | 0.22 | 6.77 |
| DS-4 | 25 | 65 | 24 | 79 | 2.81 | 4.07 | 3.78 | 6.85 |

**Table 5**
Comparison of computational cost between using observational data from the full-bridge and single-column finite-element models.

| | Exact (Full Bridge) | Existing (Full Bridge) | Proposed (Full Bridge) | Proposed (Single Column) |
|---|---|---|---|---|
| Average Time Per Analysis (min.) | 14 | 14 | 14 | 0.6 |
| Num. of Analyses Required | 160 | 79* | 25* | 50 |
| Total Computation Time (min.) | 2240 | 948 | 350 | 30 |
| % Reduction Compared with Single Column | 98.7% | 96.8% | 91.4% | – |

* Average number of analyses required for four damage states.

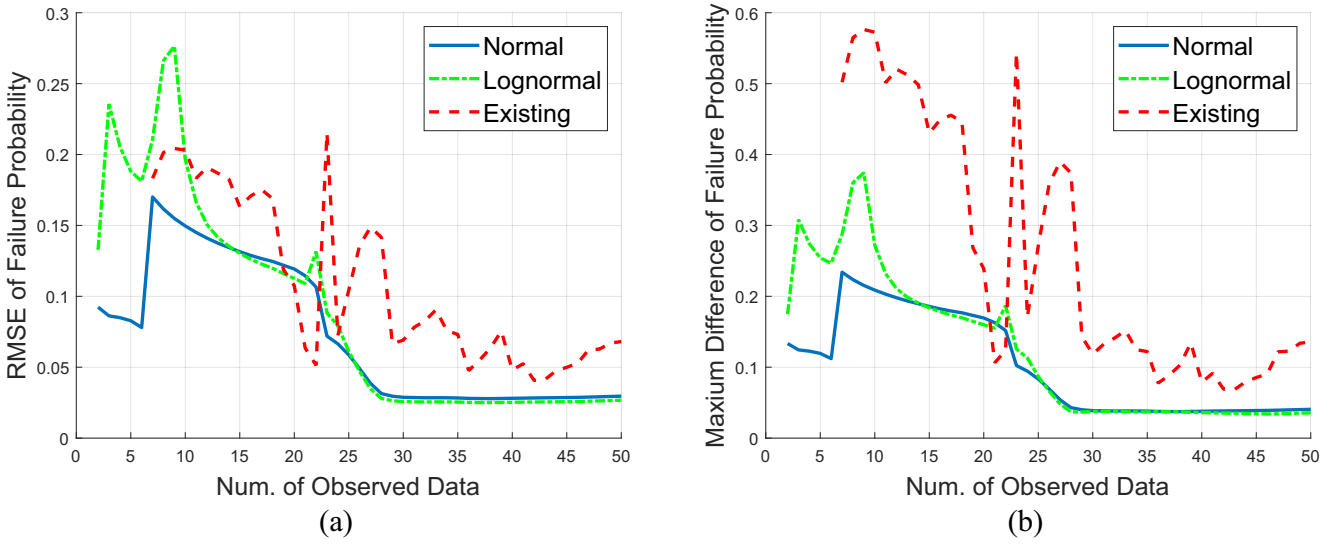


**Fig. 13.** (a) RMSE and (b) maximum difference of failure probability for DS-4 with 20% mass loss.

20% mass loss using normal compared with lognormal prior distributions. Results are shown in Fig. 13.

The results show that both distribution types converge to a similar level of accuracy, e.g., once the number of observed data points reaches 25 in this case. However, the assumption of a normal distribution for the prior distributions leads overall to more accurate fragility estimations, particularly when fewer numbers of observed data are available.

## Declaration of Competing Interest

The authors declare that they have no known competing financial interests or personal relationships that could have appeared to influence the work reported in this paper.

## Acknowledgements

This project was partially funded by the INSPIRE University Transportation Center (UTC). Financial support for INSPIRE UTC projects is provided by the U.S. Department of Transportation, Office of the Assistant Secretary for Research and Technology (USDOT/OST-R) under Grant No. 69A3551747126 through INSPIRE University Transportation Center (http://inspire-utc.mst.edu) at Missouri University of Science and Technology. The views, opinions, findings and conclusions reflected in this publication are solely those of the authors and do not represent the official policy or position of the USDOT/OST-R, or any State or other entity.

## References

[1] Almusallam AA. Effect of degree of corrosion on the properties of reinforcing steel bars. Constr Build Mater 2001;15(8):361–8.
[2] Meda A, Mostosi S, Rinaldi Z, Riva P. Experimental Evaluation of the corrosion influence on the cyclic behavior of RC columns. Eng Struct 2014;76:112–23.
[3] Apostolopoulos CA, Papadopoulos MP, Pantelakis SG. Tensile behavior of corroded reinforcing steel bars BSt 500s. Constr Build Mater 2006;20 (9):782–9.
[4] Ang AH, Tang WH. Probability concepts in engineering planning and design: Basic principles, Vol. I. New York: Wiley; 1975.
[5] Argyroudis SA, Mitoulis SA, Winter MG, Kaynia AM. Fragility of transport assets exposed to multiple hazards: State-of-the-art review toward infrastructural resilience. Reliab Eng Syst Saf 2019;191:106567.
[6] Argyroudis SA, Mitoulis SA, Chatzi E, Baker JW, Brilakis I, Gkoumas K, et al. Digital technologies can enhance global climate resilience of critical infrastructure. *Climate*. Risk Management 2021;100387.
[7] Baker JW. Efficient analytical fragility function fitting using dynamic structural analysis. Earthquake Spectra 2015;31(1):579–99.
[8] Bavirisetty R, Vinayagamoorthy M, Duan L. Dynamic Analysis, Bridge Engineering – Seismic Design, Edited by Wai-Fah Chen and Lian Duan, CRC Press LLC, Boca Raton, FL, ISBN: 0-8493-1683-9/02; 2003.
[9] Billah AHM, Alam M. Seismic fragility assessment of highway bridges: a state-of-the-art review. Struct Infrastruct Eng 2015;11(6):804–32.
[10] Capé M. Residual service-life assessment of existing R/C structures. Goteborg (Sweden) and Milan University of Technology, Italy Erasmus Program: In Chalmers University of Technology; 1999.
[11] Chiou B, Darragh R, Gregor N, Silva W. NGA project strong-motion database. Earthquake Spectra 2008;24(1):23–44.
[12] Choe D, Gardoni P, Rosowsky D. Closed-form fragility estimates, parameter sensitivity, and bayesian updating for RC columns. J Eng Mech 2007;133 (7):833–43.
[13] Choi E. Seismic analysis and retrofit of Mid-America bridges. Georgia: School of Civil and Environmental Engineering, Georgia Institute of Technology; 2002. Ph.D. thesis.
[14] Choi E, DesRoches R, Nielson BG. Seismic fragility of typical bridges in moderate seismic zones. Eng Struct 2004;26:187–99.
[15] Coleman J, Spacone E. Localization issues in force-based frame elements. J Struct Eng 2001;127(11):1257–65.
[16] Cornell AC, Jayaler F, Hamburger RO, Foutch AD. Probabilistic Basis for 2000 SAC Federal Emergency Management Agency Steel Moment Frame Guidelines. J Struct Eng 2002;128(4):526–33.
[17] Coronelli D, Gambarova P. Structural assessment of corroded reinforced concrete beams: modeling guidelines. J Struct Eng 2004;130(8):1214–24.
[18] Der Kiureghian A. Bayesian methods for seismic fragility assessment of lifeline components. In: Kiureghian AD (Ed.), Acceptable risk processes: Lifelines and natural hazards, Monograph No. 21. Reston, VA: Technical Council for Lifeline Earthquake Engineering, ASCE; 2002.
[19] Dong Y, Frangopol DM. Probabilistic time-dependent multihazard life-cycle assessment and resilience of bridges considering climate change. J Perform Constr Facil 2016;30(5):04016034.
[20] Du YG, Clark LA, Chan AHC. Residual capacity of corroded reinforcing bars. Mag Concr Res 2005;57(3):135–47.
[21] Du YG, Clark LA, Chan AHC. Effect of corrosion on ductility of reinforcing bars. Mag Concr Res 2005;57(7):407–19.
[22] Ellingwood BR, Hwang H. Probabilistic Descriptions of Resistance of Safety-Related Structures in Nuclear Plants. Nucl Eng Des 1985;88(2):169–78.
[23] Ellingwood BR. Earthquake risk assessment of building structures. Reliab Eng Syst Saf 2001;74(3):251–62.
[24] Gardoni P, Der Kiureghian A, Mosalam KM. Probabilistic capacity models and fragility estimates for reinforced concrete columns based on experimental observations. ASCE J Eng Mech 2002; 128, 1024–1038.
[25] Kashani MM, Crewe AJ, Alexander NA. Use of a 3D optical measurement technique for stochastic corrosion pattern analysis of reinforcing bars subjected to accelerated corrosion. Corros Sci 2013;73:208–21.
[26] Kashani MM, Lowes LN, Crewe AJ, Alexander NA. Phenomenological hysteretic model for corroded reinforcing bars including inelastic buckling and low-cycle fatigue degradation. Comput Struct 2015;156:58–71.
[27] Broomfield J. Corrosion of steel in concrete: understanding. In: investigation and repair. Crc Press; 2003.
[28] Kashani, MM, Lowes LN, Crewe AJ, Alexander NA. Computational modelling strategies for nonlinear response prediction of corroded circular RC bridge piers. Adv Mater Sci Eng; 2016.
[29] Ghosh J, Padgett JE. Aging considerations in the development of time-dependent seismic fragility curves. J Struct Eng 2010;136(12):1497–511.

[30] Hwang H, Liu JB, Chiu YH. Seismic fragility analysis of highway bridges. Mid-America Earthquake Center CD Release 2001:01–6.
[31] Jacinto L. *Safety assessment of existing bridges. Bayesian probabilistic approach* (PhD thesis). FCT/UNL (in Portuguese); 2011.
[32] Kiani J, Camp C, Pezeshk S. On the application of machine learning techniques to derive seismic fragility curves. Comput Struct 2019;218:108–22.
[33] Koutsourelakis PS. Assessing structural vulnerability against earthquakes using multi-dimensional fragility surfaces: A Bayesian framework. Probab Eng Mech 2010;25:49–60.
[34] Lallemant D, Kiremidjian A, Burton H. Statistical procedures for developing earthquake damage fragility curves. Earthquake Eng Struct Dyn 2015;44(9):1373–89.
[35] Li J, Spencer BF, Elnashai AS. Bayesian updating of fragility functions using hybrid simulation. ASCE J Struct Eng 2012;139:1160–71.
[36] Luco N, Cornell CA. Effects of random connection fractures on the demands and reliability for a three-story pre-Northridge (SMRP) structure. Oakland, California: Earthquake Engineering Research Institute; 1998.
[37] Lunn D, Jackson C, Best N, Spiegelhalter D, Thomas A. The BUGS book: A practical introduction to Bayesian analysis. Chapman and Hall/CRC; 2012.
[38] Mackie K, Stojadinovic B. Fragility basis for california highway overpass bridge seismic decision making, (PEER Report 2005/02). Pacific Earthquake Engineering Research Center. Berkeley, CA: University of California; 2005.
[39] Mander JB, Priestley MJ, Park R. Theoretical stress-strain model for confined concrete. J Struct Eng 1988;114(8):1804–26.
[40] McKay MD, Conover WJ, Beckman RJ. A comparison of three methods for selecting values of input variables in the analysis of output from a computer code. Technometrics 1979;21:239–45.
[41] Megally SH, Silva PF, Seible F. *Seismic Response of Sacrificial Shear Keys in Bridge Abutments*, Structural Systems Research Project SSRP-2001/24. San Diego, La Jolla, CA: University of California; 2002.
[42] Melchers RE. Structural Reliability Analysis and Prediction. second edition. West Sussex, England: John Wiley & Sons Ltd.; 2001.
[43] Mitropoulou CC, Papadrakakis M. Developing fragility curves based on neural network IDA predictions. Eng Struct 2011;33(12):3409–21.
[44] Molina FJ, Alonso C, Andrade C. Cover cracking as a function of rebar corrosion: part 2—numerical model. Mater Struct 1993;26(9):532–48.
[45] Nielson BG. Analytical fragility curves for highway bridges in moderate seismic zones (Doctoral dissertation, Georgia Institute of Technology); 2005.
[46] Nielson BG, DesRoches R. Seismic fragility methodology for highway bridges using a component level approach. Earthquake Eng Struct Dyn 2007;36:823–39.
[47] Noh HY, Kiremidjian A, Ceferino L, So E. Bayesian updating of earthquake vulnerability functions with application to mortality rates. Earthquake spectra 2017;33(3):1173–89.
[48] Padgett JE. Seismic vulnerability assessment of retrofitted bridges using probabilistic methods. Atlanta, GA: Georgia Institute of Technology; 2007. Ph. D. Dissertation.
[49] Ramanathan K, DesRoches R, Padgett JE. A comparison of pre- and post-seismic design considerations in moderate seismic zones through the fragility assessment of multi-span bridge classes. Eng Struct 2012;45:559–73.
[50] Ramanathan, K. Next generation seismic fragility curves for California bridges incorporating the evolution in seismic design philosophy, Ph.D. Dissertation. Georgia Institute of Technology, Atlanta, GA; 2012.
[51] Sacks R, Girolami M, Brilakis I. Building information modelling, artificial intelligence and construction tech. Develop Built Environ 2020;4:100011.
[52] Sainct R, Feau C, Martinez JM, Garnier J. Efficient methodology for seismic fragility curves estimation by active learning on Support Vector Machines. Struct Saf 2020;86:101972.
[53] Shamsabadi A, Yan L. *Closed-Form Force-Displacement Backbone Curves for Bridge Abutment Backfill Systems*, Proceedings of the Geotechnical Earthquake Engineering and Soil Dynamics IV Congress. American Society of Civil Engineers; 2008.
[54] Shang F, An X, Mishima T, Maekawa K. Three-dimensional nonlinear bond model incorporating transverse action in corroded RC members. J Adv Concr Technol 2011;9(1):89–102.
[55] Shinozuka M, Feng MQ, Kim H-K, Kim S-H. Nonlinear static procedure for fragility curve development. ASCE J Eng Mech 2000;126:1287–96.
[56] Singhal A, Kiremidjian AS. Bayesian updating of fragilities with application to RC frames. J Struct Eng 1998;124(8):922–9.
[57] Thanapol Y, Akiyama M, Frangopol DM. Updating the seismic reliability of existing RC structures in a marine environment by incorporating the spatial steel corrosion distribution: application to bridge piers. J Bridge Eng 2016;21(7):04016031.
[58] Vamvatsikos D, Cornell AC. Incremental dynamic analysis. Earthquake Eng Struct Dyn 2002;31:491–514.
[59] Vecchio FJ, Collins MP. The modified compression-field theory for reinforced concrete elements subjected to shear. ACI J 1986;83(2):219–31.
[60] Ou Y-C, Tsai L-L, Chen H-H. Cyclic performance of large-scale corroded reinforced concrete beams. Earthquake Eng Struct Dyn 2012;41(4):593–604.
[61] Ma Y, Che Y, Gong J. Behavior of corrosion damaged circular reinforced concrete columns under cyclic loading. Constr Build Mater 2012;29:548–56.
[62] Zhang J, Huo Y. Evaluating effectiveness and optimum design of isolation devices for highway bridges using the fragility function method. Eng Struct 2009;31:1648–60.
[63] Zhong J, Gardoni P, Rosowsky D, Haukaas T. Probabilistic seismic demand models and fragility estimates for reinforced concrete bridges with two-column bents. J Eng Mech 2008;134(6):495–504.
[64] Zhang Y, DesRoches R, Tien I. Impact of corrosion on risk assessment of shear-critical and short lap-spliced bridges. Eng Struct 2019;189:260–71.
[65] Zhang Y, Tien I. Methodology for Regularization of Force-Based Elements to Model Reinforced Concrete Columns with Short Lap Splices. J Eng Mech 2020;146(7):04020073.
[66] Zhang Y, Tien I. Methodology to account for the impact of stress history in layered soils for seismic vulnerability assessment of scoured bridges. Struct Infrastruct Eng 2020:1–24.
[67] Zhao J, Sritharan S. Modeling of strain penetration effects in fiber-based analysis of reinforced concrete structures. ACI Mater J 2007;104(2):133.
[68] Scott BD, Park R, Priestley MJN. Stress-strain behavior of concrete confined by overlapping hoops at low and high strain rates. Journal of the American Concrete Institute 1982;79(1):13–27.
[69] McKenna Francis Thomas. Object-oriented finite element programming: frameworks for analysis, algorithms and parallel computing. Berkeley: University of California; 1997.